UCLA
COMPUTATIONAL AND APPLIED MATHEMATICS

Non-oscillatory Central Schemes for Multidimensional Hyperbolic Conservation Laws

Guang-Shan Jiang
Eitan Tadmor

October 1996

CAM Report 96-36

Department of Mathematics
University of California, Los Angeles
Los Angeles, CA. 90024-1555

Non-oscillatory Central Schemes for Multidimensional Hyperbolic Conservation Laws

Guang-Shan Jiang[†] Eitan Tadmor[†‡]

September 30, 1996

Abstract

We construct, analyze and implement a new non-oscillatory high-resolution scheme for two-dimensional Hyperbolic conservation laws. The scheme is a predictor-corrector method which consists of two-steps: starting with given cell averages, we first predict pointvalues which are based on non-oscillatory piecewise-linear reconstructions from the given cell averages; at the second corrector step, we use *staggered* averaging, together with the predicted midvalues, to realize the evolution of these averages. This results in a second-order, non-oscillatory *central* scheme – a natural extension of the one-dimensional second-order central scheme of Nessyahu & Tadmor [NT].

As in the one-dimensional case, the main feature of our two-dimensional scheme is *simplicity*. In particular, this central scheme does not require the intricate and time consuming (approximate) Riemann solvers which are essential for the high-resolution upwind schemes; in fact, even the computation of the exact Jacobians can be avoided. Moreover, the central scheme is 'genuinely multidimensional' in the sense that it does not necessitate dimensional splitting.

We prove that the scheme satisfies the *scalar maximum principle*, and in the more general context of systems, our proof indicates that the scheme is *positive* (in the sense of Lax & Liu [LL]). We demonstrate the application of our central scheme to several prototype two-dimensional Euler problems. Our numerical experiments include the resolution of shocks oblique to the computational grid; they show how our central scheme solves with high resolution the intricate wave interactions in the so called double Mach reflection problem, [WC], *without* following the characteristics; and finally we report on the accurate ray solutions of a weakly Hyperbolic system, [ER], rays which otherwise are missed by dimensional splitting approach. Thus, a considerable amount of simplicity and robustness is gained while achieving stability and high-resolution.

AMS(MOS) subject classification. Primary 65M10; Secondary 65M05

Keywords. Hyperbolic conservation laws, multidimensional systems, central difference schemes, non-oscillatory schemes.

[†]Department of Mathematics, UCLA, Los-Angeles CA 90095.
[‡]School of Mathematical Sciences, Tel-Aviv University, Tel-Aviv 69978 Israel

Contents

1 Introduction

We study the approximation of two-dimensional conservation laws by second-order accurate, non-oscillatory *central* difference schemes. The main feature of our central schemes is *simplicity*: since no (approximate) Riemann solvers and related characteristic decompositions are involved, we derive efficient, genuinely multidimensional schemes, which are independent of dimensional splitting.

The construction of our central scheme in the prototype two-dimensional case is carried out in §2. It amounts to a simple two-step predictor-corrector method outlined in (2.15)-(2.16) below. In §3 we carry out the stability analysis which proves that the two-dimensional scheme satisfies the *scalar maximum principle*. In fact, our arguments indicate that in the more general context of multidimensional *systems*, the central scheme satisfies the *positivity condition* of Lax & Liu, [LL]. Finally, we implemented the proposed central scheme for a variety of prototype two-dimensional problems, whose results are reported in §4. In particular, we would like to highlight

- Scalar equations. The non-oscillatory behavior of the scalar results are found in agreement with the maximum principle indicated above;

- Two-dimensional systems. Three canonical problems are considered – the rotated Riemann problem, the Double Mach reflection problem, and a 2×2 *weakly* Hyperbolic system introduced by Engquist & Runborg, which arises in the macroscopic closure of a multi-phase geometrical optics expansion, [ER]. The numerical results demonstrate the non-oscillatory, high-resolution content of our proposed central schemes. It is in this context of *systems* of conservation laws that the simplicity and flexibility of our central schemes are translated into *efficiency*. Specifically, one can avoid the time consuming computation of (approximate) Riemann-solver(s) and the related characteristic decompositions – in fact, even the (exact) Jacobians

associated with the problem are not required for the computation!. Moreover, this flexibility enables to implement the central scheme *without* dimensional splitting.

The motivation for our construction of the two-dimensional central scheme discussed in this paper, originates with the one-dimensional central scheme introduced by **Nessyahu & Tadmor** in [NT]. To begin with, we briefly recall this one-dimensional setup. Starting with a piecewise-constant solution, $\sum \bar{w}_p^n \chi_p(x)$, one reconstructs a piecewise-linear approximation, $w(x,t^n) = \sum \left[\bar{w}_p^n + w_p' \left(\frac{x-x_p}{\Delta x}\right)\right] \chi_p(x)$. Here, $\chi_p(x)$ is characteristic function of the cell, $I_p := \{\xi \,\big|\, |\xi - x_p| \le \frac{\Delta x}{2}\}$, centered around $x_p = p\Delta x$, and w_p' abbreviates a first-order discrete slope which is reconstructed from the neighboring cell averages $\{\bar{w}_q^n\}$. Let $\{w(x,t),\ t \ge t^n\}$, be the exact solution of the conservation law $w_t + f(w)_x = 0$, subject to the *reconstructed* initial data at $t = t^n$; the distinctive feature of central schemes — in contrast to Godunov-type upwind schemes, is that they realize this exact solution by its averages over *staggered* cells, $I_{j+\frac{1}{2}}$, centered around $x_{j+\frac{1}{2}} = \left(j+\frac{1}{2}\right)\Delta x$. Let $\bar{w}_{j+\frac{1}{2}}(t) := \frac{1}{\Delta x}\int_{I_{j+\frac{1}{2}}} w(\xi,t)d\xi$ denote these staggered averages. Integration over the control volume $I_{j+\frac{1}{2}} \times [t^n, t^{n+1}]$ yields (- with the usual fixed mesh-ratio $\lambda := \frac{\Delta t}{\Delta x}$)

$$\bar{w}_{j+\frac{1}{2}}(t^{n+1}) = \bar{w}_{j+\frac{1}{2}}(t^n) - \lambda\left[\frac{1}{\Delta t}\int_{t^n}^{t^{n+1}} f(w_{j+1}(\tau))d\tau - \frac{1}{\Delta t}\int_{t^n}^{t^{n+1}} f(w_j(\tau))d\tau\right].$$

The averaging of the piecewise-linear data reconstructed at $t = t^n$ yields $\bar{w}_{j+\frac{1}{2}}(t^n) = \frac{1}{2}(w_j^n + w_{j+1}^n) + \frac{1}{8}(w_j' - w_{j+1}')$. So far everything is *exact*. At this point the fluxes on the right are *approximated* by the midpoint rule, $\frac{1}{\Delta t}\int_{t^n}^{t^{n+1}} f(w_j(\tau))d\tau \sim f(w_j(t^{n+\frac{1}{2}}))$. The CFL condition guarantees that the interface values, $w_j(\tau) = w(x_j,\tau), \tau \in [t^n, t^{n+1})$, are 'secured' within a smooth region, so one may use Taylor expansion to approximate the midvalue $w_j(t^{n+\frac{1}{2}})$. We end up with a predictor step for these midvalues,

$$w_j^{n+\frac{1}{2}} = \bar{w}_j^n - \frac{\lambda}{2}(f(w_j))', \tag{1.1}$$

followed by the corrector step described above

$$\bar{w}_{j+\frac{1}{2}}^{n+1} = \frac{1}{2}(\bar{w}_j^n + \bar{w}_{j+1}^n) + \frac{1}{8}(w_j' - w_{j+1}') - \lambda\left[f(w_{j+1}^{n+\frac{1}{2}}) - f(w_j^{n+\frac{1}{2}})\right]. \tag{1.2}$$

Here, w_j', and likewise, $f(w_j)'$, denote spatial *discrete slopes* of the corresponding grid functions. There is a variety of recepies for the construction of such slopes, e.g., [Sw],[LO]. These discrete slopes involve nonlinear limiters, which guarantee that the central scheme (1.1)-(1.2) is non-oscillatory in the sense described below.

Acknowledgment. Research was supported by DARPA/ONR Grant #N00014-92-J-1890 and ONR Grant #N0014-91-J1076.

1.1 One-dimensional epilogue – no characteristic decompositions

The scalar central scheme (1.1)-(1.2) shares desirable non-oscillatory properties with the scalar high-resolution *upwind* schemes. In this context we refer to proofs of total-

variation bounds (– the TVD property, [Ha2]), entropy stability (– cell entropy inequality, [OT]), maximum principle, etc., consult [NT],[Hu],[LT]. The distinctive advantage of the central schemes, however, is due to their non-oscillatory behavior with *systems* of conservation laws. Specifically, the *vector* of discrete slopes required in the corrector step (1.2), w'_j, is now implemented using a straightforward *componentwise* extension of the scalar recepies. In particular, for the discrete derivative of the flux in the predictor step (1.1), we may use $f(w_j)' = A(w_j)w'_j$; alternatively, we can proceed with a straightforward *componentwise* computation of $f(w_j)'$, which does not even require the Jacobian, $A = f_w$. In either case, intricate and time consuming characteristic decompositions of upwind differencing are avoided – a straightforward componentwise approach will do for the central scheme (1.1)-(1.2).

These advantages of the central framework were already borne out in several related works of , e.g., [BS], [Er], [Hu], [LT], [NT], [Sa2], [TW]. Here we provide one more simple demonstration of this point in the context of the one-dimensional, constant-coefficients test system proposed to us by **Engquist & Osher**, [EO],

$$u_t + (Au)_x = 0, \qquad A := \begin{pmatrix} 0 & 1 \\ 1 & 0 \end{pmatrix}, \tag{1.3}$$

subject to discontinuous initial data (and periodic boundary conditions)

$$\begin{aligned} u_1(x,0) &\equiv 1 \\ u_2(x,0) &= \begin{cases} 1, & x < 0, \\ 0, & x > 0. \end{cases} \end{aligned} \tag{1.4}$$

Careful numerical simulations are required to model the the propagation of such initial singularities. Let us recall that post processing and artificial compression of contact discontinuities, e.g. [MO], [Ha1], are just two remedies to the spurious oscillations which are formed in connection with the numerical simulations of such singularities. Figure 1.1 compares the results of the central scheme (1.1)-(1.2) using the MinMod limiter MM_θ outlined in (3.1′), with those of the upwind ENO-ROE scheme outlined in [JS]. Both schemes used *componentwise* reconstructions of pointvalues from cell averages. Figures 1.1(a)-(b) demonstrate that the central scheme is able to perfectly resolve the discontinuities carried by each of the characteristic variables, $v_1 := u_1 + u_2$ and $v_2 := u_1 - u_2$, *without* spurious oscillations in the other characteristic variable. One can detect such oscillations, however, in the second-order upwind results of Figure 1.1(c), oscillations which become more pronounced in the third-order results of Figure 1.1(d). This type of behavior repeated itself in a variety of test cases we have tried with different systems and stronger jump amplitudes.

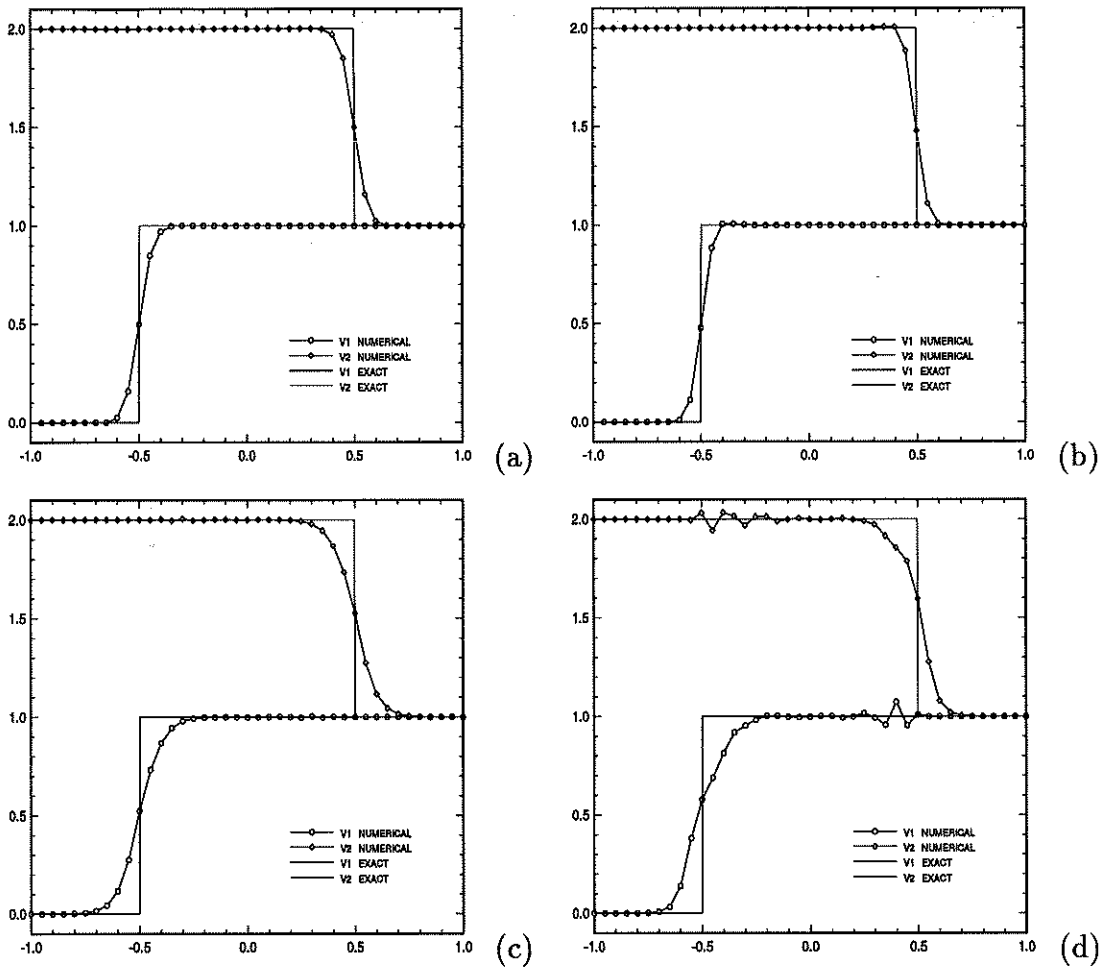

Figure 1.1: The 2×2 system (1.3)-(1.4) evaluated with $N = 40$ cells and CFL=0.4 at $t = 0.5$. Plotted are numerical and exact characteristic variables. Nessyahu-Tadmor NT scheme (1.1)-(1.2) with MinMod limiter in (3.1′): (a) with MM_1 limiter; (b) with MM_2 limiter. Results are compared with ENO-ROE scheme: (c) Componentwise 2nd order ENO-ROE; (d) Componentwise 3rd order ENO-ROE.

2 The two-dimensional central scheme

2.1 A two-step predictor-corrector formulation

We consider the two-dimensional system of conservation laws

$$u_t + f(u)_x + g(u)_y = 0, \tag{2.1}$$

subject to prescribed initial data, $u(x, y, t = 0) = u_0(x, y)$. To approximate (2.1) by a central scheme, we begin with a piecewise constant solution of the form $\sum \bar{w}^n_{pq} \chi_{pq}(x, y)$. Here, $\bar{w}^n_{pq}$ is the approximate cell average at $t = t^n$, associated with the cell $C_{pq} = I_p \times J_q$ centered around $(x_p = p\Delta x, y_q = q\Delta y)$, i.e., $C_{pq} := \left\{ (\xi, \eta) \,\middle|\, |\xi - x_p| \le \frac{\Delta x}{2},\ |\eta - y_q| \le \frac{\Delta y}{2} \right\}$.

As a first step, we *reconstruct* a piecewise-linear approximation of the form

$$w(x,y,t^n)=\sum\left[\bar{w}^n_{pq}+w'_{pq}\left(\frac{x-x_p}{\Delta x}\right)+w_{pq}^{\backprime}\left(\frac{y-y_q}{\Delta y}\right)\right]\chi_{pq}(x,y). \tag{2.2}$$

Here, w'_{pq} and $w_{pq}^{\backprime}$ are *discrete slopes* in the x- and, respectively, y-direction, which are reconstructed from the given cell averages. To guarantee second order accuracy, these slopes should approximate the corresponding derivatives,

$$w'_{pq}\sim\Delta x\cdot w_x(x_p,y_q,t^n)+\mathcal{O}(\Delta x)^2 \tag{2.3$'$}$$

$$w_{pq}^{\backprime}\sim\Delta y\cdot w_y(x_p,y_q,t^n)+\mathcal{O}(\Delta y)^2. \tag{2.3$^{\backprime}$}$$

As in the one-dimensional framework, the construction of our central scheme proceeds with a second step of an exact evolution followed by staggered averaging.

Let $\{w(x,y,t),\ t\geq t^n\}$, be the exact solution of the conservation law (2.1),

$$w_t+f(w)_x+g(w)_y=0,\quad t\geq t^n, \tag{2.4}$$

subject to the reconstructed piecewise-linear data (2.2), $w(x,y,t^n)$, at $t=t^n$. The second (and distinctive) step is to realize this exact solution at the next time step $t=t^{n+1}$, by its averages over *staggered* cells, $C_{j+\frac{1}{2},k+\frac{1}{2}}:=I_{j+\frac{1}{2}}\times J_{k+\frac{1}{2}}$, centered around $(x_{j+\frac{1}{2}},y_{k+\frac{1}{2}})$.

Let $\bar{w}_{j+\frac{1}{2},k+\frac{1}{2}}(t)=\fint_{C_{j+\frac{1}{2},k+\frac{1}{2}}}w(x,y,t)dxdy$ denote these staggered averages. (Here and below we abbreviate $\fint_B:=\frac{1}{|B|}\int_B$ to denote the *normalized* integral – normalized over its length, area...). Let $\lambda:=\frac{\Delta t}{\Delta x}$ and $\mu:=\frac{\Delta t}{\Delta y}$ denote the fixed mesh-ratios. Integration of (2.4) over $C_{j+\frac{1}{2},k+\frac{1}{2}}\times[t^n,t^{n+1})$ yields

$$\begin{aligned}\bar{w}_{j+\frac{1}{2},k+\frac{1}{2}}(t^{n+1}) &= \fint_{C_{j+\frac{1}{2},k+\frac{1}{2}}}w(x,y,t^n)dxdy+\\ &-\lambda\left\{\fint_{\tau=t^n}^{t^{n+1}}\fint_{y\in J_{k+\frac{1}{2}}}\left[f(w(x_{j+1},y,\tau))-f(w(x_j,y,\tau))\right]dyd\tau\right\}+\\ &-\mu\left\{\fint_{\tau=t^n}^{t^{n+1}}\fint_{x\in I_{j+\frac{1}{2}}}\left[g(w(x,y_{k+1},\tau))-g(w(x,y_k,\tau))\right]dxd\tau\right\}.\end{aligned} \tag{2.5}$$

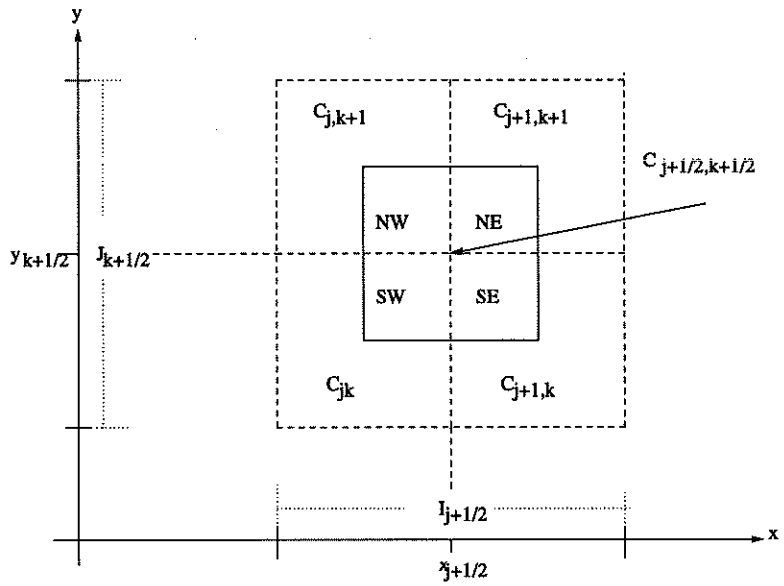

Figure 2.1: Floor plan of the staggered grid.

We begin by evaluating the cell average, $\fint_{C_{j+\frac{1}{2},k+\frac{1}{2}}} w(x,y,t^n)dxdy$. It has contributions from the four intersecting cells, $C_{jk}, C_{j+1,k}, C_{j+1,k+1}$ and $C_{j,k+1}$. Starting with the intersecting cell C_{jk} at the South West corner – consult figure 2.1, $C^{SW}_{j+\frac{1}{2},k+\frac{1}{2}} := C_{j+\frac{1}{2},k+\frac{1}{2}} \cap C_{jk}$, we find the average of the reconstructed polynomial in (2.2),

$$\begin{aligned}\fint_{C^{SW}_{j+\frac{1}{2},k+\frac{1}{2}}} w(x,y,t^n)dxdy &= \\ &= \fint_{x_j}^{x_{j+\frac{1}{2}}}\fint_{y_k}^{y_{k+\frac{1}{2}}}\left[\bar{w}^n_{jk} + w'_{jk}\left(\frac{x-x_j}{\Delta x}\right) + w_{jk}^{\backprime}\left(\frac{y-y_k}{\Delta y}\right)\right]dxdy = \\ &= \frac{1}{4}\bar{w}^n_{jk} + \frac{1}{16}(w'_{jk} + w_{jk}^{\backprime}). \qquad (2.6)\end{aligned}$$

Continuing in a counterclockwise direction, we have

$$\fint_{C^{SE}_{j+\frac{1}{2},k+\frac{1}{2}}} w(x,y,t^n)dxdy = \frac{1}{4}\bar{w}^n_{j+1,k} + \frac{1}{16}(-w'_{j+1,k} + w_{j+1,k}^{\backprime}), \qquad (2.7)$$

$$\fint_{C^{NE}_{j+\frac{1}{2},k+\frac{1}{2}}} w(x,y,t^n)dxdy = \frac{1}{4}\bar{w}^n_{j+1,k+1} - \frac{1}{16}\left(w'_{j+1,k+1} + w_{j+1,k+1}^{\backprime}\right), \qquad (2.8)$$

$$\fint_{C^{NW}_{j+\frac{1}{2},k+\frac{1}{2}}} w(x,y,t^n)dxdy = \frac{1}{4}\bar{w}^n_{j,k+1} + \frac{1}{16}\left(w'_{j,k+1} - w_{j,k+1}^{\backprime}\right). \qquad (2.9)$$

By adding the last four integrals we find the exact staggered averages of the reconstructed solution at $t = t^n$,

$$\bar{w}^n_{j+\frac{1}{2},k+\frac{1}{2}} := \fint_{C_{j+\frac{1}{2},k+\frac{1}{2}}} w(x,y,t^n)dxdy = \qquad (2.10)$$

$$= \frac{1}{4}(\bar{w}^n_{jk} + \bar{w}^n_{j+1,k} + \bar{w}^n_{j,k+1} + \bar{w}^n_{j+1,k+1}) +$$
$$+ \frac{1}{16}\Big\{(w'_{jk} - w'_{j+1,k}) + (w'_{j,k+1} - w'_{j+1,k+1}) + (w\backprime_{jk} - w\backprime_{j,k+1}) + (w\backprime_{j+1,k} - w\backprime_{j+1,k+1})\Big\}.$$

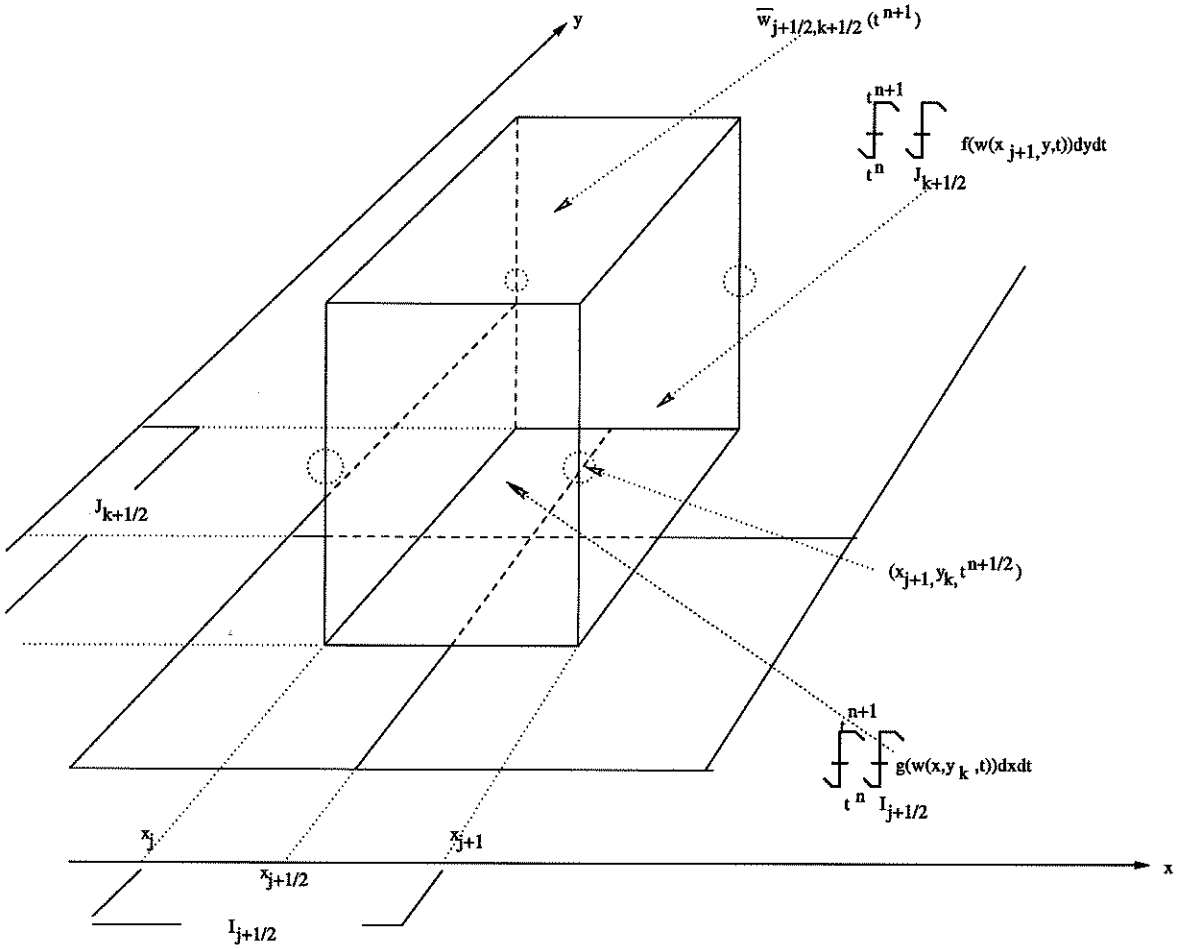

Figure 2.2: The central, staggered stencil.

So far everything is *exact*. We now turn to *approximate* the four fluxes on the right of (2.5), starting with the one along the East face, consult figure 2.2, $\fint_{t^n}^{t^{n+1}} \fint_{J_{k+\frac{1}{2}}} f(w(x_{j+1}, y, \tau))dyd\tau$. We use the midpoint quadrature rule for second-order approximation of the temporal integral, $\fint_{y\in J_{k+\frac{1}{2}}} f(w(x_{j+1}, y, t^{n+\frac{1}{2}}))dy$; and, for reasons to be clarified below, we use the second-order rectangular quadrature rule for the spatial integration across the y-axis,

yielding

$$\int_{t^n}^{t^{n+1}} \int_{y\in J_{k+\frac{1}{2}}} f(w(x_{j+1},y,\tau))dyd\tau \sim \frac{1}{2}\left[f(w^{n+\frac{1}{2}}_{j+1,k}) + f(w^{n+\frac{1}{2}}_{j+1,k+1})\right]. \tag{2.11}$$

In a similar manner we approximate the remaining fluxes,

$$\int_{t^n}^{t^{n+1}} \int_{x\in I_{j+\frac{1}{2}}} g(w(x,y_{k+1},\tau))dxd\tau \sim \frac{1}{2}\left[g(w^{n+\frac{1}{2}}_{j,k+1}) + g(w^{n+\frac{1}{2}}_{j+1,k+1})\right] \tag{2.12}$$

$$\int_{t^n}^{t^{n+1}} \int_{y\in J_{k+\frac{1}{2}}} f(w(x_j,y,\tau))dyd\tau \sim \frac{1}{2}\left[f(w^{n+\frac{1}{2}}_{jk}) + f(w^{n+\frac{1}{2}}_{j,k+1})\right], \tag{2.13}$$

$$\int_{t^n}^{t^{n+1}} \int_{x\in I_{j+\frac{1}{2}}} g(w(x,y_k,\tau))dxd\tau \sim \frac{1}{2}\left[g(w^{n+\frac{1}{2}}_{jk}) + g(w^{n+\frac{1}{2}}_{j+1,k})\right]. \tag{2.14}$$

The approximate fluxes in (2.11) - (2.14) make use of the midpoint values, $w^{n+\frac{1}{2}}_{jk} \equiv w(x_j,y_k,t^{n+\frac{1}{2}})$, and it is here that we take advantage of utilizing these midvalues for the spatial integration by the rectangular rule. Namely, since these midvalues are secured at the smooth center of their cells, C_{jk}, bounded away from the jump discontinuities along the edges, we may use Taylor expansion, $w(x_j,y_k,t^{n+\frac{1}{2}}) = \bar{w}^n_{jk} + \frac{\Delta t}{2}w_t(x_j,y_k,t^n) + \mathcal{O}(\Delta t)^2$. Finally, we use the conservation law (2.4) to express the time derivative, w_t, in terms of the spatial derivatives, $f(w)'$ and $g(w)\backprime$,

$$w^{n+\frac{1}{2}}_{jk} = \bar{w}^n_{jk} - \frac{\lambda}{2}f(w)'_{jk} - \frac{\mu}{2}g(w)\backprime_{jk}. \tag{2.15}$$

Here, $f(w)'_{jk} \sim \Delta x \cdot f(w(x_j,y_k,t^n))_x$ and $g(w)\backprime_{jk} \sim \Delta y \cdot g(w(x_j,y_k,t^n))_y$, are one-dimensional discrete slopes in the x- and y-directions, of the type reconstructed in (2.3′); for example, multiplication of (2.3′)-(2.3\) by the corresponding Jacobians A and B yields

$$f(w)'_{jk} = A(\bar{w}^n_{jk})w'_{jk}, \qquad g(w)\backprime_{jk} = B(\bar{w}^n_{jk})w\backprime_{jk}.$$

Equipped with the midvalues (2.15), we can now evaluate the approximate fluxes (2.11-2.14). Inserting these values, together with the staggered average computed in (2.11), into (2.5), we conclude with new staggered averages at $t = t^{n+1}$, given by

$$\begin{aligned}
\bar{w}^{n+1}_{j+\frac{1}{2},k+\frac{1}{2}} &= \frac{1}{4}(\bar{w}^n_{jk} + \bar{w}^n_{j+1,k} + \bar{w}^n_{j,k+1} + \bar{w}^n_{j+1,k+1}) + \\
&+ \frac{1}{16}(w'_{jk} - w'_{j+1,k}) - \frac{\lambda}{2}\left[f(w^{n+\frac{1}{2}}_{j+1,k}) - f(w^{n+\frac{1}{2}}_{j,k})\right] \\
&+ \frac{1}{16}(w'_{j,k+1} - w'_{j+1,k+1}) - \frac{\lambda}{2}\left[f(w^{n+\frac{1}{2}}_{j+1,k+1}) - f(w^{n+\frac{1}{2}}_{j,k+1})\right] \\
&+ \frac{1}{16}(w\backprime_{jk} - w\backprime_{j,k+1}) - \frac{\mu}{2}\left[g(w^{n+\frac{1}{2}}_{j,k+1}) - g(w^{n+\frac{1}{2}}_{j,k})\right] \\
&+ \frac{1}{16}(w\backprime_{j+1,k} - w\backprime_{j+1,k+1}) - \frac{\mu}{2}\left[g(w^{n+\frac{1}{2}}_{j+1,k+1}) - g(w^{n+\frac{1}{2}}_{j+1,k})\right].
\end{aligned} \tag{2.16}$$

In summary, we end up with a simple two-step predictor-corrector scheme (2.15) - (2.16). Starting with the cell averages, $\bar{w}^n_{jk}$, we use the first-order predictor (2.15) for the evaluation of the midpoint values, $w^{n+\frac{1}{2}}_{jk}$, which is followed by the second-order corrector (2.16) for the computation of the new cell averages, $\bar{w}^{n+1}_{jk}$. This results in a second-order accurate non-oscillatory scheme. As in the one-dimensional case – no (approximate) Riemann solvers are involved – the non-oscillatory behavior of the scheme hinges on the reconstructed discrete slopes, $w', w\backprime, f(w)'$ and $g(w)\backprime$.

2.2 A one-dimensional-like formulation revisited

The corrector step (2.16) bares a close similarity with the one-dimensional corrector formula (1.2). Indeed, let us introduce the notation for staggered averaging in the x- and y-directions,

$$< \omega_{j,\cdot} >_{k+\frac{1}{2}} := \frac{1}{2}(\omega_{jk} + \omega_{j,k+1}), \quad < \omega_{\cdot,k} >_{j+\frac{1}{2}} := \frac{1}{2}(\omega_{jk} + \omega_{j+1,k}).$$

Then (2.16) takes the simple one-dimensional-like form (compare the one-dimensional corrector in (1.2))

$$\begin{aligned} \bar{w}^{n+1}_{j+\frac{1}{2},k+\frac{1}{2}} &= < \frac{1}{2}(\bar{w}^n_{j,\cdot} + \bar{w}^n_{j+1,\cdot}) + \frac{1}{8}(w'_{j,\cdot} - w'_{j+1,\cdot}) - \lambda[f(w^{n+\frac{1}{2}}_{j+1,\cdot}) - f(w^{n+\frac{1}{2}}_{j,\cdot})] >_{k+\frac{1}{2}} + \\ &+ < \frac{1}{2}(\bar{w}^n_{\cdot,k} + \bar{w}^n_{\cdot,k+1}) + \frac{1}{8}(w\backprime_{\cdot,k} - w\backprime_{\cdot,k+1}) - \mu[g(w^{n+\frac{1}{2}}_{\cdot,k+1}) - g(w^{n+\frac{1}{2}}_{\cdot,k})] >_{j+\frac{1}{2}} . \end{aligned}$$

3 The maximum principle for scalar approximations

It is well-known that the exact entropy solution of the *scalar* conservation law (2.1) satisfies a maximum principle. In this section we prove that under appropriate CFL condition, our central scheme (2.15)-(2.16) satisfies the same maximum principle. To this end, it is essential to reconstruct the discrete slopes, w' and $w\backprime$, with built in *limiters*, which we now briefly describe in the context of the prototype example

$$w'_{jk} = MM\{\theta(\bar{w}^n_{j+1,k} - \bar{w}^n_{j,k}), \frac{1}{2}(\bar{w}^n_{j+1,k} - \bar{w}^n_{j-1,k}), \theta(\bar{w}^n_{j,k} - \bar{w}^n_{j-1,k})\} \qquad (3.1')$$

$$w\backprime_{jk} = MM\{\theta(\bar{w}^n_{j,k+1} - \bar{w}^n_{j,k}), \frac{1}{2}(\bar{w}^n_{j,k+1} - \bar{w}^n_{j,k-1}), \theta(\bar{w}^n_{j,k} - \bar{w}^n_{j,k-1})\}. \qquad (3.1\backprime)$$

Here, the choice $\theta = 1$ coincides with the 'classical' so-called Min-Mod limiter, e.g. [Ha1],[Sw]; it guarantees that the corresponding piecewise linear reconstruction in (2.2), $w(x, y, t^n)$, is *co-monotone* with the underlying piecewise constant approximation, $\sum \bar{w}^n_{pq}\chi_{pq}$. The range of θ's, $1 \le \theta \le 2$, allows for a further variety of accurate reconstructions which satisfy the maximum principle, $\|w(\cdot, t^n)\|_{L^\infty} \le \|\sum \bar{w}^n_{pq}\chi_{pq}(\cdot)\|_{L^\infty}$. The essential feature in the definition of these discrete slopes, however, is due to the Min-Mod (MM) function:

its output equals the input variable with minimal modules among all its input variables, unless the latter disagree in sign in which case $MM = 0$,

$$MM\{v_1, v_2, \ldots\} = \begin{cases} \min_p \{v_p\} & \text{if } v_p > 0, \ \forall p \\ \max_p \{v_p\} & \text{if } v_p < 0, \ \forall p \\ 0 & \text{otherwise} \end{cases}$$

In particular, the so called *clipping phenomena* may occur, due to the reconstruction of zero discrete slopes at extrema cells (– where forward and backward differences change signs). The feature of clipping limiter is clearly necessary to retain the maximum principle at the reconstruction step. It implies that the neighboring discrete slopes cannot have *opposite* signs, and in particular

$$|w'_{j+1,k} - w'_{j,k}| \leq \max(|w'_{j+1,k}|, |w'_{j,k}|) \leq \theta |\bar{w}_{j+1,k} - \bar{w}_{j,k}|, \quad 1 \leq \theta < 2, \tag{3.2}$$

$$|w\backprime_{j,k+1} - w\backprime_{j,k}| \leq \max(|w\backprime_{j,k+1}|, |w\backprime_{j,k}|) \leq \theta |\bar{w}_{j,k+1} - \bar{w}_{j,k}|, \quad 1 \leq \theta < 2. \tag{3.3}$$

Similar estimates apply to the reconstructed discrete slopes for the flux; for example

$$|f(w)'_{j+1,k} - f(w)'_{jk}| \leq \max(|f(w)'_{j+1,k}|, |f(w)'_{jk}|) \leq \theta |f(\bar{w}^n_{j+1,k}) - f(\bar{w}^n_{jk})|. \tag{3.4}$$

Theorem 1 *Consider the two-dimensional scalar scheme (2.15-2.16). Assume that the discrete slopes, w' and $w\backprime$, satisfy the (θ-dependent) limiter property (3.2-3.3), and likewise for $f(w)'$ and $g(w)\backprime$ (– e.g., the minmod limiter (3.1'-3.1\backprime)). Then for any $\theta < 2$ there exists a sufficiently small CFL number, C_θ (– e.g. $C_1 = (\sqrt{7} - 2)/6 \sim 0.1$), such that if the CFL condition is fulfilled,*

$$\max(\lambda \cdot \max_u |f_u(u)|, \mu \cdot \max_u |g_u(u)|) \leq C_\theta,$$

then the following local maximum principle holds

$$|\bar{w}^{n+1}_{j+\frac{1}{2},k+\frac{1}{2}}| \leq \max\{|\bar{w}^n_{jk}|, |\bar{w}^n_{j+1,k}|, |\bar{w}^n_{j,k+1}|, |\bar{w}^n_{j+1,k+1}|\} \tag{3.5}$$

Proof. Our key observation is to rewrite the new value computed in (2.16), $\bar{w}^{n+1}_{j+\frac{1}{2},k+\frac{1}{2}}$, as the average of four distinctive terms

$$\begin{aligned} \bar{w}^{n+1}_{j+\frac{1}{2},k+\frac{1}{2}} &= \frac{1}{4} \times \\ &\Big\{ \frac{1}{2}\left(\bar{w}^n_{jk} + \bar{w}^n_{j+1,k}\right) + \frac{1}{4}\left(w'_{jk} - w'_{j+1,k}\right) - 2\lambda\left(f^{n+\frac{1}{2}}_{j+1,k} - f^{n+\frac{1}{2}}_{j,k}\right) + \\ &+ \frac{1}{2}\left(\bar{w}^n_{j,k+1} + \bar{w}^n_{j+1,k+1}\right) + \frac{1}{4}\left(w'_{j,k+1} - w'_{j+1,k+1}\right) - 2\lambda\left(f^{n+\frac{1}{2}}_{j+1,k+1} - f^{n+\frac{1}{2}}_{j,k+1}\right) + \\ &+ \frac{1}{2}\left(\bar{w}^n_{jk} + \bar{w}^n_{j,k+1}\right) + \frac{1}{4}\left(w\backprime_{jk} - w\backprime_{j,k+1}\right) - 2\mu\left(g^{n+\frac{1}{2}}_{j,k+1} - g^{n+\frac{1}{2}}_{jk}\right) + \\ &+ \frac{1}{2}\left(\bar{w}^n_{j+1,k} + \bar{w}^n_{j+1,k+1}\right) + \frac{1}{4}\left(w\backprime_{j+1,k} - w\backprime_{j+1,k+1}\right) - 2\mu\left(g^{n+\frac{1}{2}}_{j+1,k+1} - g^{n+\frac{1}{2}}_{j+1,k}\right) \Big\} \\ &=: \frac{1}{4} \times \{\mathcal{I}_1 + \mathcal{I}_2 + \mathcal{I}_3 + \mathcal{I}_4\}. \end{aligned} \tag{3.6}$$

Here and below we abbreviate, $f_{jk}^{n+\frac{1}{2}} = f(\bar{w}_{jk}^{n+\frac{1}{2}})$.
We will show that each of these four terms, $\mathcal{I}_j$, can be written as an appropriate sum of the cell averages at t^n, $\{\bar{w}_{jk}^n, \bar{w}_{j+1,k}^n, \bar{w}_{j,k+1}^n, \bar{w}_{j+1,k+1}^n\}$, so that $\bar{w}_{j+\frac{1}{2},k+\frac{1}{2}}^{n+1}$ can be expressed as a *convex* combination of these averages. This implies, in particular, that the local maximum principle (3.5) holds.

We begin by estimating the difference between two neighboring midvalues, say $w_{j+1,k}^{n+\frac{1}{2}} - w_{jk}^{n+\frac{1}{2}}$, evaluated in the predictor step (2.15)

$$\begin{aligned} w_{j+1,k}^{n+\frac{1}{2}} - w_{jk}^{n+\frac{1}{2}} &= \bar{w}_{j+1,k}^n - \bar{w}_{jk}^n + \\ &- \frac{\lambda}{2}[f(w)'_{j+1,k} - f(w)'_{jk}] - \frac{\mu}{2}[g(w)'_{j+1,k} - g(w)'_{jk}]. \end{aligned} \tag{3.7}$$

Since by (3.4), $f(w)'_{j+1,k}$ and $f(w)'_{jk}$ cannot have opposite signs, their differences on the right of (3.7) does not exceed

$$|f(w)'_{j+1,k} - f(w)'_{jk}| \le \theta |f(\bar{w}_{j+1,k}^n) - f(\bar{w}_{jk}^n)| \le \theta \mathsf{a} |\bar{w}_{j+1,k}^n - \bar{w}_{jk}^n|. \tag{3.8}$$

Here and below, $\mathsf{a} := \max_u |f_u(u)|$ and $\mathsf{b} := \max_u |g_u(u)|$ denote the maximal speeds in the x- and y-directions. The third difference on the right of (3.7), $g(w)'_{j+1,k} - g(w)'_{jk}$, represents a 'mixed' derivative (which allows for opposite signs); here we use the straightforward (3.1')

$$\begin{aligned} |g(w)'_{j+1,k} - g(w)'_{jk}| &\le |g(w)'_{j+1,k}| + |g(w)'_{jk}| \le \\ &\le \theta \left[|g(\bar{w}_{j+1,k+1}^n) - g(\bar{w}_{j+1,k}^n)| + |g(\bar{w}_{j,k+1}^n) - g(\bar{w}_{jk}^n)| \right] \\ &\le \theta \mathsf{b} \left[|\bar{w}_{j,k+1}^n - \bar{w}_{jk}^n| + |\bar{w}_{j+1,k+1}^n - \bar{w}_{j+1,k}^n| \right]. \end{aligned} \tag{3.9}$$

Using (3.8) and (3.9) we obtain an upperbound on the midvalues difference in (3.7), which in turn, enables us to upperbound the corresponding flux difference

$$\begin{aligned} \lambda |f_{j+1,k}^{n+\frac{1}{2}} - f_{jk}^{n+\frac{1}{2}}| &\le \lambda \mathsf{a} |w_{j+1,k}^{n+\frac{1}{2}} - w_{jk}^{n+\frac{1}{2}}| \le \\ &\le \frac{1}{2} \lambda \mathsf{a} (2 + \theta \cdot \lambda \mathsf{a}) |\bar{w}_{j+1,k}^n - \bar{w}_{jk}^n| + \\ &+ \frac{1}{2} \theta \cdot \lambda \mathsf{a} \cdot \mu \mathsf{b} \left[|\bar{w}_{j,k+1}^n - \bar{w}_{jk}^n| + |\bar{w}_{j+1,k+1}^n - \bar{w}_{j+1,k}^n| \right]. \end{aligned} \tag{3.10}$$

We now return to the first term, $\mathcal{I}_1$, in (3.6): by (3.2) and (3.10), it does not exceed

$$\begin{aligned} |\mathcal{I}_1| \le \frac{1}{2} |\bar{w}_{jk}^n + \bar{w}_{j+1,k}^n| &+ \left(\frac{\theta}{4} + \lambda \mathsf{a} \left(2 + \theta \cdot \lambda \mathsf{a} \right) \right) |\bar{w}_{j+1,k}^n - \bar{w}_{jk}^n| + \\ &+ \theta \cdot \lambda \mathsf{a} \cdot \mu \mathsf{b} |\bar{w}_{j,k+1}^n - \bar{w}_{jk}^n| + \theta \cdot \lambda \mathsf{a} \cdot \mu \mathsf{b} |\bar{w}_{j+1,k+1}^n - \bar{w}_{j+1,k}^n|. \end{aligned}$$

Thus

$$|\mathcal{I}_1| \le \mathcal{I}_{11} + \mathcal{I}_{12} + \mathcal{I}_{13} + \mathcal{I}_{14} \tag{3.11}$$

where

$$\begin{aligned}\mathcal{I}_{11} &= \frac{1}{2}|\bar{w}^n_{jk}+\bar{w}^n_{j+1,k}|, \quad \mathcal{I}_{12}=\alpha_{\lambda \mathsf{a}}|\bar{w}^n_{j+1,k}-\bar{w}^n_{jk}|, \qquad \alpha_{\lambda \mathsf{a}}:=\frac{\theta}{4}+\lambda \mathsf{a}\,(2+\theta\cdot\lambda \mathsf{a})\\ \mathcal{I}_{13} &= \beta|\bar{w}^n_{j,k+1}+\bar{w}^n_{jk}|, \quad \mathcal{I}_{14}=\beta|\bar{w}^n_{j+1,k+1}-\bar{w}^n_{j+1,k}|, \quad \beta:=\theta\cdot\lambda \mathsf{a}\cdot\mu \mathsf{b}.\end{aligned}$$

In a similar manner we obtain

$$\begin{aligned}|\mathcal{I}_2| &\le \frac{1}{2}|\bar{w}^n_{j,k+1}+\bar{w}^n_{j+1,k+1}|+\alpha_{\lambda a}|\bar{w}^n_{j+1,k+1}-\bar{w}^n_{j,k+1}|+ \qquad (3.12)\\ &+ \beta|\bar{w}^n_{j,k+1}-\bar{w}^n_{jk}|+\beta|\bar{w}^n_{j+1,k+1}-\bar{w}^n_{j+1,k}|=:\mathcal{I}_{21}+\mathcal{I}_{22}+\mathcal{I}_{23}+\mathcal{I}_{24};\\ |\mathcal{I}_3| &\le \frac{1}{2}|w^n_{jk}+\bar{w}^n_{j,k+1}|+\alpha_{\mu b}|\bar{w}^n_{j,k+1}-\bar{w}^n_{jk}|+ \qquad (3.13)\\ &+ \beta|\bar{w}^n_{j+1,k}-\bar{w}^n_{jk}|+\beta|\bar{w}^n_{j+1,k+1}-\bar{w}^n_{j,k+1}|=:\mathcal{I}_{31}+\mathcal{I}_{32}+\mathcal{I}_{33}+\mathcal{I}_{34}\end{aligned}$$

and finally

$$\begin{aligned}|\mathcal{I}_4| &\le \frac{1}{2}|\bar{w}^n_{j+1,k}+\bar{w}^n_{j+1,k+1}|+\alpha_{\mu b}|\bar{w}^n_{j+1,k+1}-\bar{w}^n_{j+1,k}|+ \qquad (3.14)\\ &+ \beta|\bar{w}^n_{j+1,k}-\bar{w}^n_{j,k}|+\beta|\bar{w}^n_{j+1,k+1}-\bar{w}^n_{j,k+1}|=:\mathcal{I}_{41}+\mathcal{I}_{42}+\mathcal{I}_{43}+\mathcal{I}_{44}.\end{aligned}$$

We now conclude by re-grouping similar terms in the last four bounds; specifically, we rearrange the summation of the last four bounds in (3.11-3.14),

$$\sum_{j=1}^{4}\mathcal{I}_j=(\mathcal{I}_{11}+\mathcal{I}_{12}+\mathcal{I}_{33}+\mathcal{I}_{43})+(\mathcal{I}_{21}+\mathcal{I}_{22}+\mathcal{I}_{34}+\mathcal{I}_{44})+\cdots$$

and we obtain

$$\begin{aligned}|\bar{w}^{n+1}_{j+\frac{1}{2},k+\frac{1}{2}}| &\le \frac{1}{4}\sum_{j=1}^{4}|\mathcal{I}_j|\le\frac{1}{4}\times\\ &\Big\{\ \frac{1}{2}|\bar{w}^n_{jk}+\bar{w}^n_{j+1,k}|+(\alpha_{\lambda a}+2\beta)|\bar{w}^n_{j+1,k}-\bar{w}^n_{jk}|+\\ &+\ \frac{1}{2}|\bar{w}^n_{j,k+1}+\bar{w}^n_{j+1,k+1}|+(\alpha_{\lambda a}+2\beta)|\bar{w}^n_{j+1,k+1}-\bar{w}^n_{j,k+1}|+\\ &+\ \frac{1}{2}|\bar{w}^n_{jk}+\bar{w}^n_{j,k+1}|+(\alpha_{\mu b}+2\beta)|\bar{w}^n_{j,k+1}-\bar{w}^n_{jk}|+\\ &+\ \frac{1}{2}|\bar{w}^n_{j+1,k}+\bar{w}^n_{j+1,k+1}|+(\alpha_{\mu b}+2\beta)|\bar{w}^n_{j+1,k+1}-\bar{w}^n_{j+1,k}|\Big\}.\end{aligned}$$

Our assertion concerning the convex combination – and hence of the local maximum principle follows, provided the following inequalities hold:

$$\alpha_{\lambda \mathsf{a}}+2\beta \equiv \frac{\theta}{4}+\lambda \mathsf{a}\,(2+\theta\cdot\lambda \mathsf{a}+2\theta\cdot\mu \mathsf{b})\le\frac{1}{2} \qquad (3.15)$$

$$\alpha_{\mu b}+2\beta \equiv \frac{\theta}{4}+\mu \mathsf{b}\,(2+\theta\cdot\mu \mathsf{b}+2\theta\cdot\lambda \mathsf{a})\le\frac{1}{2}; \qquad (3.16)$$

Clearly, for any $\theta<2$, these inequalities are satisfied for sufficiently small CFL number, $\lambda \mathsf{a}+\mu \mathsf{b}$. For example, for the 'canonical' MinMod limiter (with $\theta=1$), we find that (3.15-3.16) hold provided $\max(\lambda \mathsf{b},\mu \mathsf{b})$ does not exceed the largest root of $12\kappa^2+8\kappa-1=0$, which yields (3.5).

4 Numerical experiments. Two-dimensional high resolution

4.1 Scalar numerical results

Theorem 3.1 does not indicate the optimal CFL limitation. By measuring the wave propagation of the two-dimensional Riemann fan from the cell center at $(x_{j+\frac{1}{2}}, y_{k+\frac{1}{2}}, t^n)$ into the boundaries of that cell – consult Figure 1.1, we find the more realistic geometric CFL restriction $\max(\lambda \mathsf{a}, \mu \mathsf{b}) \leq \frac{1}{2}$. This is confirmed by the results quoted in Table 4.1, where we record the test results with simple Linear oblique advection, $u_t + u_x + u_y = 0$..

Limiter	N	L^∞ error	L^∞ order	L^1 error	L^1 order
CFL = 0.200					
MM_1	40	4.91e-2	-	1.93e-2	-
	80	2.12e-2	1.21	5.70e-3	1.76
	160	8.90e-3	1.25	1.55e-3	1.88
	320	3.70e-3	1.27	4.14e-4	1.90
MM_2	40	1.06e-2	-	6.79e-3	-
	80	2.73e-3	1.96	1.81e-3	1.91
	160	6.86e-4	1.99	4.66e-4	1.96
	320	2.35e-4	1.55	1.17e-4	1.99
UNO	40	1.08e-2	-	6.89e-3	-
	80	2.73e-3	1.98	1.74e-3	1.99
	160	6.86e-4	1.99	4.37e-4	1.99
	320	1.72e-4	2.00	1.09e-4	2.00
CFL = 0.475					
MM_1	40	4.53e-2	-	1.18e-2	-
	80	2.48e-2	0.87	6.40e-3	0.88
	160	1.92e-2	0.37	4.33e-3	0.56
	320	1.26e-1	-2.71	1.49e-2	-1.78
MM_2	40	1.34e-2	-	5.83e-3	-
	80	4.82e-3	1.48	1.74e-3	1.74
	160	1.41e-3	1.77	4.16e-4	2.06
	320	5.07e-4	1.48	1.29e-4	1.69
UNO	40	9.08e-3	-	5.80e-3	-
	80	2.74e-3	1.73	1.74e-3	1.74
	160	6.46e-4	2.08	4.11e-4	2.08
	320	1.48e-4	2.16	9.41e-5	2.13

Table 4.1: Second-order central approximation of $u_t + u_x + u_y = 0$ subject to $u_0(x, y) = \sin(\pi(x + y))$.

Here and below, we report the numerical results of the central scheme (2.15)-(2.16)

with the MM_θ-limiters in (3.1'-3.1'); both $\theta = 1$ and $\theta = 2$ were used. We also tested the Harten-Osher UNO limiter [HO]

$$w'_{jk} = MM\Big\{\Delta\bar{w}^n_{j-\frac{1}{2},k} + \frac{1}{2}MM(\Delta^2\bar{w}^n_{j-1,k}, \Delta^2\bar{w}^n_{jk}), \Delta\bar{w}^n_{j+\frac{1}{2},k} - \frac{1}{2}MM(\Delta^2\bar{w}^n_{jk}, \Delta^2\bar{w}^n_{j+1,k})\Big\}. \tag{4.1}$$

Second-order accuracy, measured in L^1-and L^∞-norms, is detected for both CFL's 0.2 and .475. As expected, the second-order accuracy with the MinMod limiters MM_1 and MM_2, deteriorated due to the clipping phenomena. The fully second order UNO limiter, however, retains the full L^1 second-order accuracy.

Next we turn to the two-dimensional Burgers' equation:

$$u_t + \frac{1}{2}(u^2)_x + \frac{1}{2}(u^2)_y = 0, \tag{4.2}$$

subject to 'oblique' initial data,

$$u_0(x,y) = \begin{cases} -1.0, & x > 0, y > 0; \\ -0.2, & x > 0, y > 0; \\ 0.5, & x < 0, y < 0; \\ 0.0, & x > 0, y < 0. \end{cases}$$

The non-oscillatory behavior of the computed solution with CFL = .475 is demonstrated in Figure 4.1. In particular, no spurious oscillations are formed, in agreement with the maximum principle proved in §3.

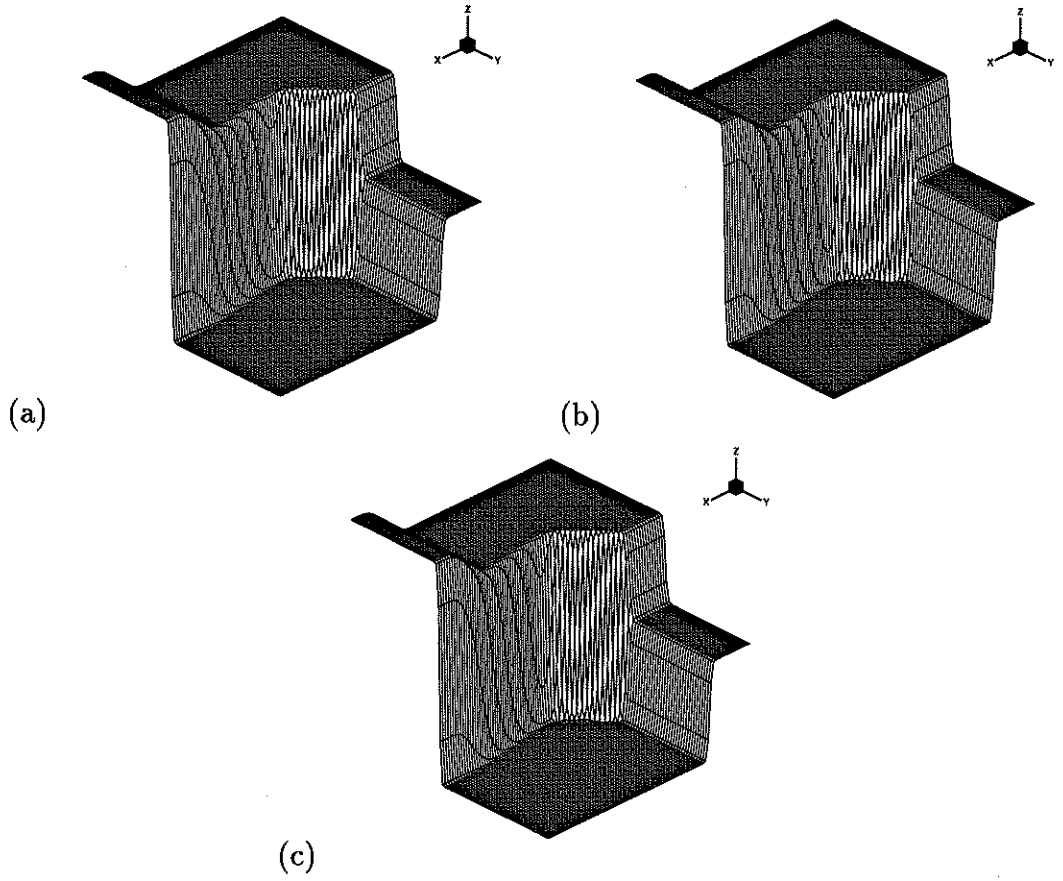

Figure 4.1: The central scheme results for Burgers' equation (4.2) evaluated with 80×80 cells and CFL=0.475 at $t = 1$. (a) with MM_1 limiter; (b) with MM_2 limiter; (c) with UNO limiter.

4.2 Efficiency and high-resolution with Hyperbolic systems

The proposed central scheme based on the predictor-corrector steps (2.15-2.16), offers a simple and robust *general purpose* approximation for two-dimensional *systems* of Hyperbolic conservation laws. In this subsection we highlight these advantages in the context of three prototype numerical experiments, governed by the two-dimensional Euler equations

$$\begin{pmatrix} \rho \\ \rho u \\ \rho v \\ E \end{pmatrix}_t + \begin{pmatrix} \rho u \\ \rho u^2 + p \\ \rho uv \\ u(E+p) \end{pmatrix}_x + \begin{pmatrix} \rho v \\ \rho uv \\ \rho v^2 + p \\ v(E+p) \end{pmatrix}_y = 0, \tag{4.3}$$

expressed in terms of the usual density, ρ, x- and y-velocities, u and v, total energy, E, and pressure, $p := (\gamma - 1)(E - \frac{1}{2}\rho(u^2 + v^2))$.

For the reader convenince, we enclose a one page Appendix with our central scheme code for the two-dimensional Euler system (4.3): The user supplies the number and size of spatial cells, the CFL number, the numerical solution at initial time "t"... (The code contains self explanatory comments). The code then evolves this solution for *two time steps* which complete a staggering cycle: regular cell $\longrightarrow$ staggered cell $\longrightarrow$ regular cell. The code can be called many times to evolve more time steps. For simplicity, the code is complemented with periodic boundary conditions in both x- and y-directions.

We begin with the **oblique Sod's problem**. Here we test the capability of our central scheme to resolve waves which are *oblique* to the computational domain. Following [JS] we initiate the two-dimensional Euler equations (4.3), with the standard one-dimensional Sod's Riemann data, [So], whose initial jump discontinuity located at $(x, y) = (2.25, 0)$, was rotated to make an angle ϕ with the x-axis – consult [JS][§8.3] for details. Figure 4.2 shows that the density at $t = 1.2$ is well resolved by the central scheme based on a computational grid of 96×16 cells and CFL=0.475. Figures 4.3 compare the fully two-dimensional computation vs. the rotated results of the one-dimensional one; thus, the errors are 'purely' due to the oblique nature of the computational waves. As is [JS], the deviations are negligible.

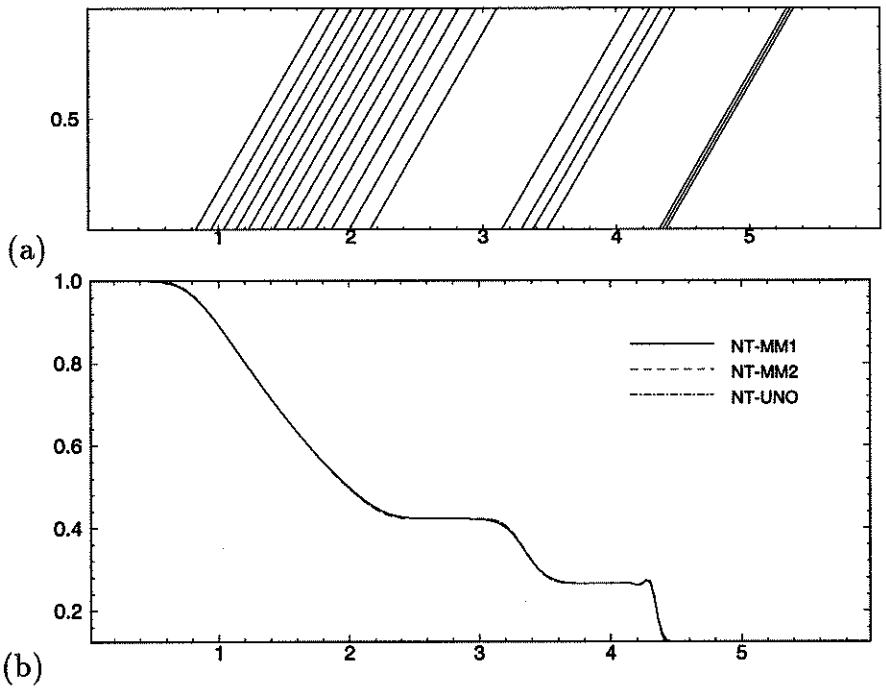

Figure 4.2: **Oblique Sod's problem computed with the central scheme: (a) Density contours computed with MM_2 limiter for initial data rotated with angle $\phi = \arctan 1$. (b) Density at $y = 0$ with rotated initial data, $\phi = \arctan 1$.**

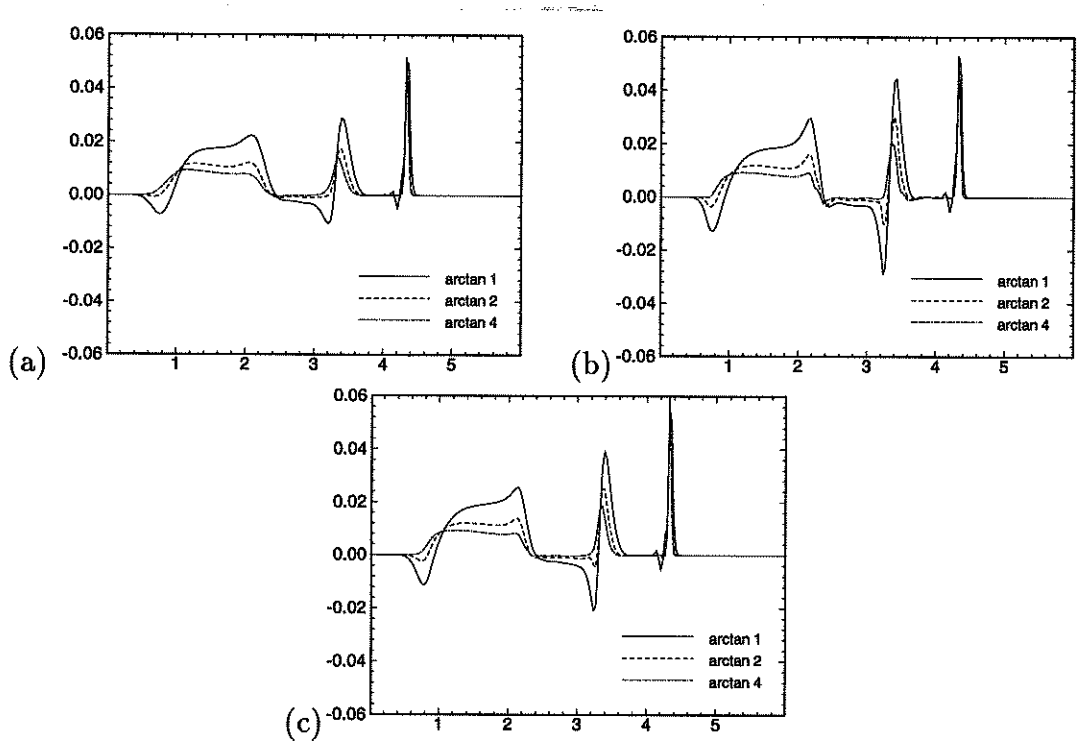

Figure 4.3: Figures (a)-(c) compare the two-dimensional oblique computation of the density, ρ_ϕ, vs. the rotated one-dimensional computation, ρ_{1D}, at $y = 0$; $\rho_\phi - \rho_{1D}$ computed with: (c) MM_1 limiter; (d) MM_2 limiter; (e) UNO limiter.

Our next example is the **double Mach reflection** problem, [WC]. The two-dimensional Euler equations (4.3), are initiated with a right-moving Mach 10 shock positioned at (x,y)=(1/6,0), and makes a 60° angle with the x-axis. The computational domain consists of the box $[0,4] \times [0,1]$. Boundary conditions: bottom boundary consists of the exact post-shock conditions at $[0,1/6]$ followed by reflective boundary conditions for the rest; at the top boundary, the flow values are set to describe the exact motion of the Mach 10 shock. We refer to [WC] for a detailed description of this problem.

Figures (4.4)-(4.6) show the numerical results of the central scheme (2.15)-(2.16), using the MinMod and UNO limiters. *It is remarkable that such a simple 'two-lines' algorithm, with no characteristic decompositions and no dimensional splitting, approximates the rather complicated double Mach reflection problem with such high resolution.* This should be compared, for example, with the higher (– forth and fifth orders) (W)ENO schemes in [JS][§8.3]. Couple of remarks are in order.

- The two-dimensional computation is more sensitive to the type of limiter than in the one-dimensional framework [NT]. In the context of the double Mach reflection problem, the MM_2 seems to yield the sharper results.

- No effort was made to optimize the boundary treatment. The staggered stencils require a different treatment for even-odd cells intersecting with the boundaries.

A more careful treatment is now studied in [TW]. The lack of boundary resolution could be observed at the bottom of the two Mach stems.

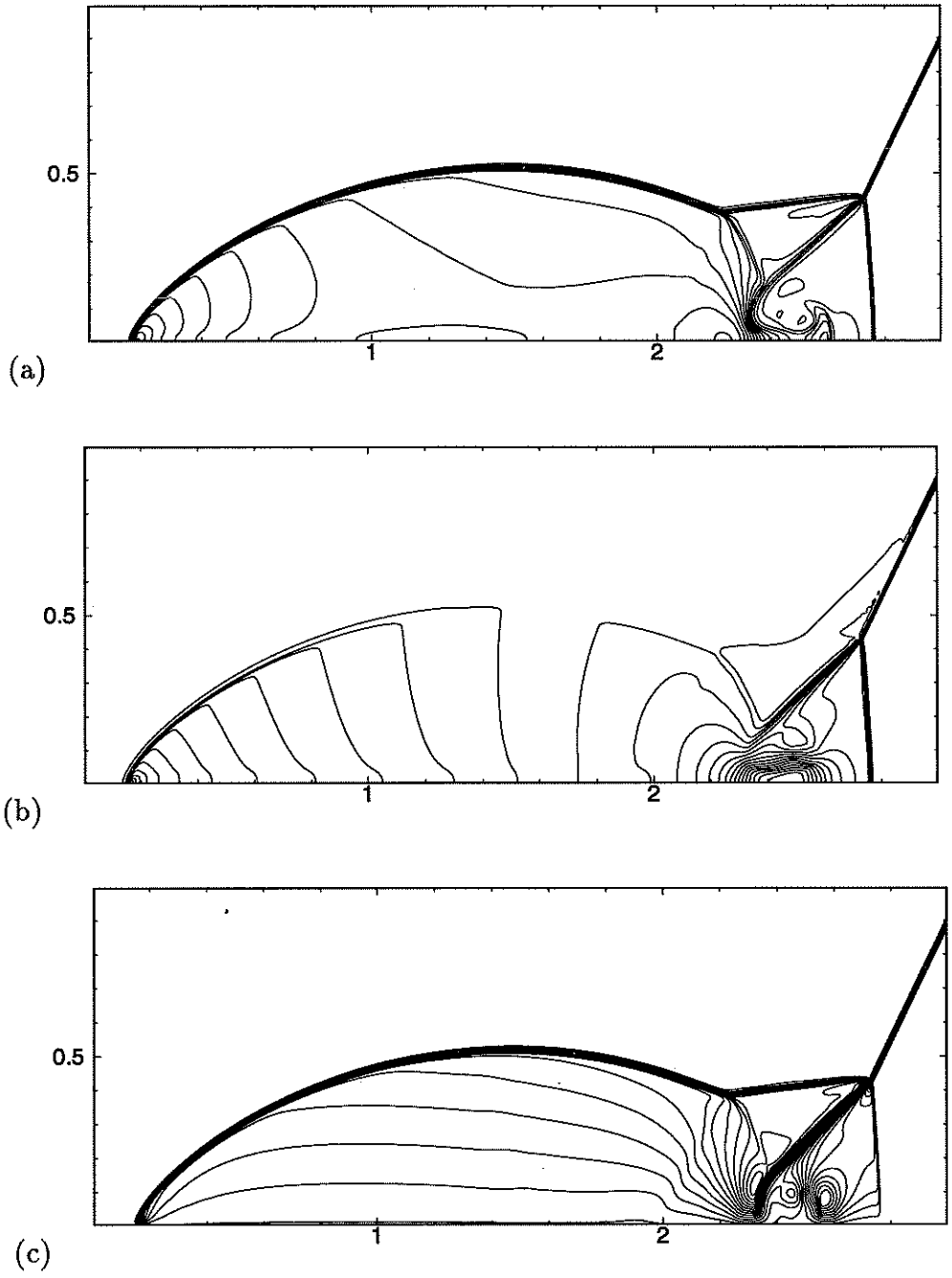

Figure 4.4: Double Mach reflection problem computed with the central scheme using MM_1 limiter with 960×240 cells and CFL=0.475 at $t = 0.2$. (a) density (b) x-velocity (c) y-velocity

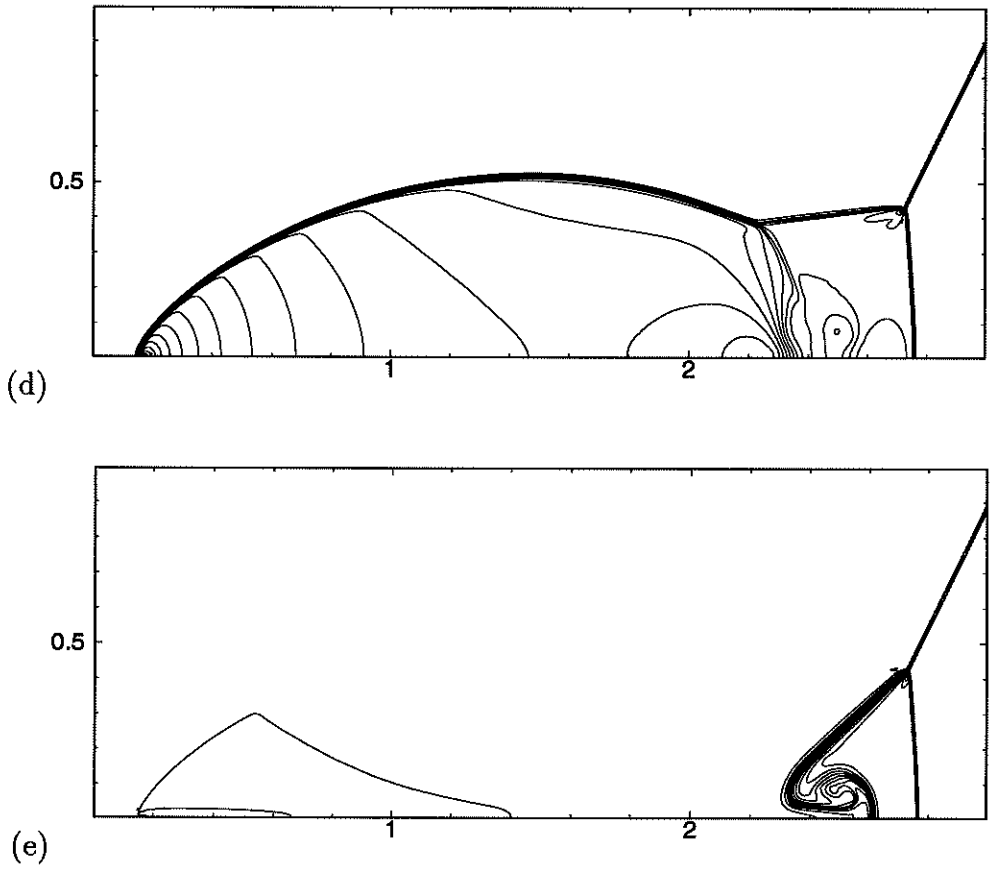

Figure 4.4: (cont'd) Double Mach reflection problem computed with the central scheme using MM_1 limiter with 960×240 cells and CFL=0.475 at $t = 0.2$ (d) pressure (e) entropy

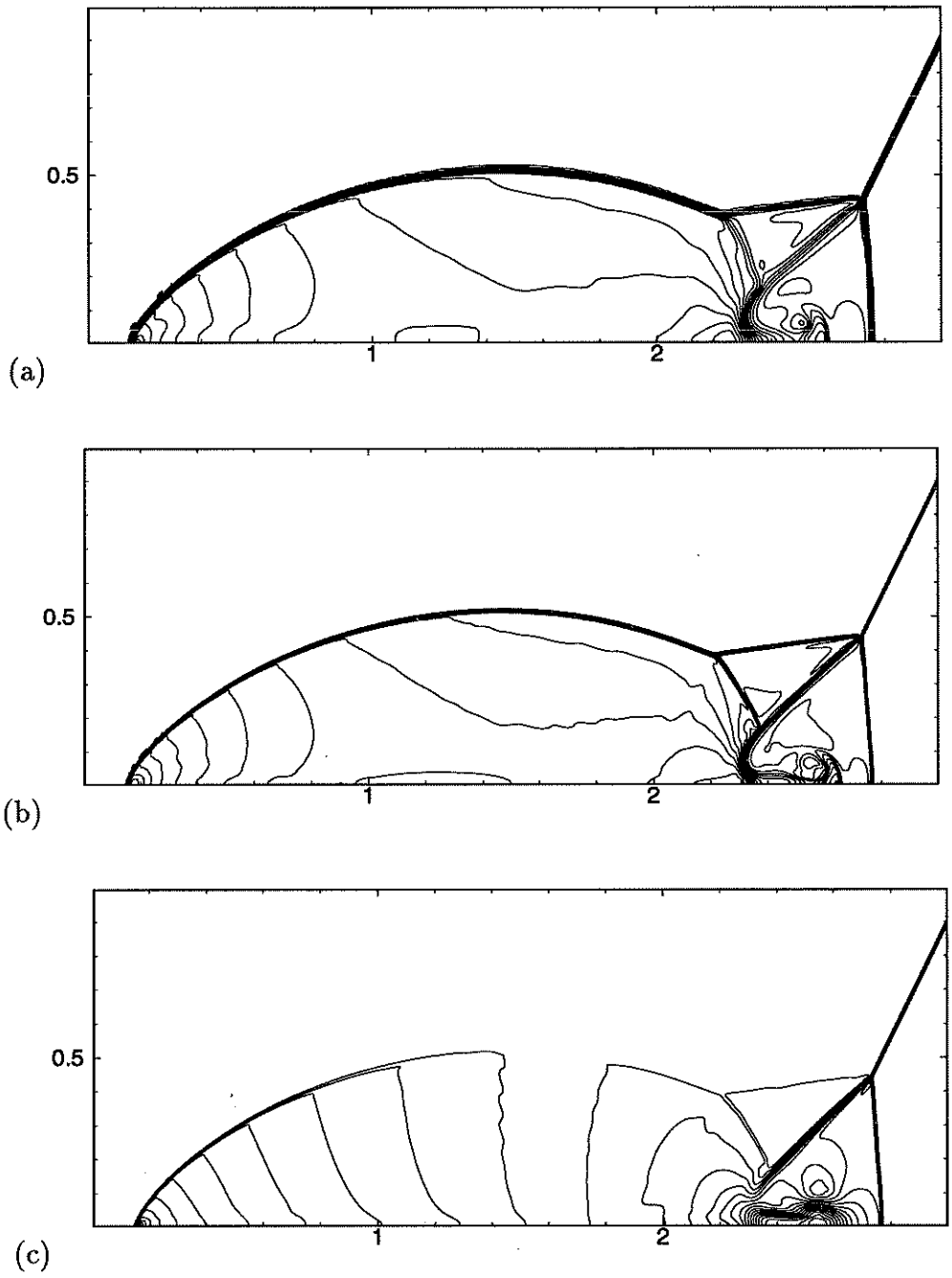

Figure 4.5: Double Mach reflection problem computed with the central scheme using MM_2 limiter with CFL=0.475 at $t = 0.2$ (a) density computed with 480×120 cells (b) density computed with 960×240 cells (c) x-velocity computed with 960×240 cells

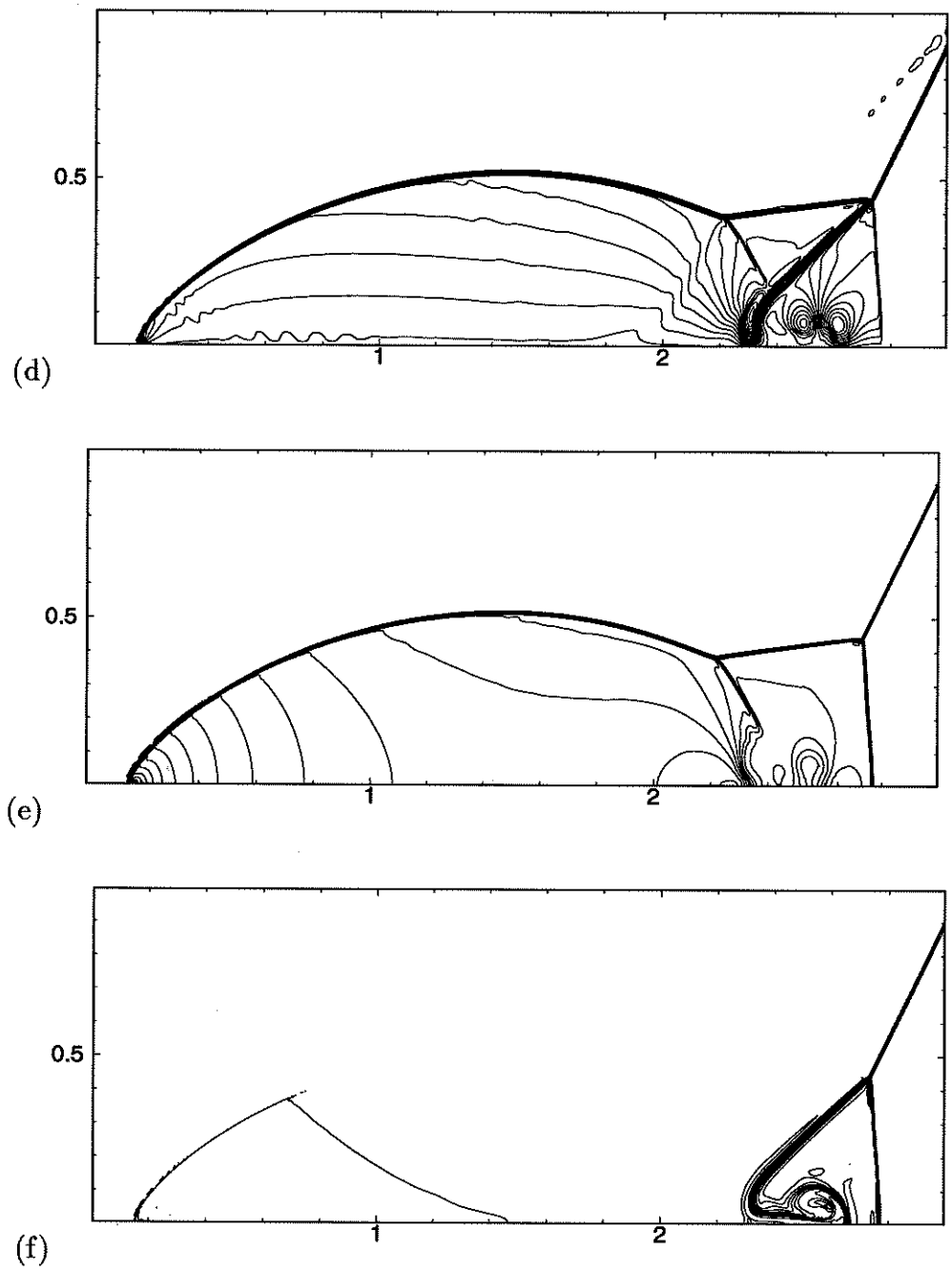

Figure 4.5: (cont'd) Double Mach reflection problem computed with the central scheme using MM_2 limiter with 960×240 cells and CFL=0.475 at $t = 0.2$ (d) y-velocity (e) pressure (f) entropy

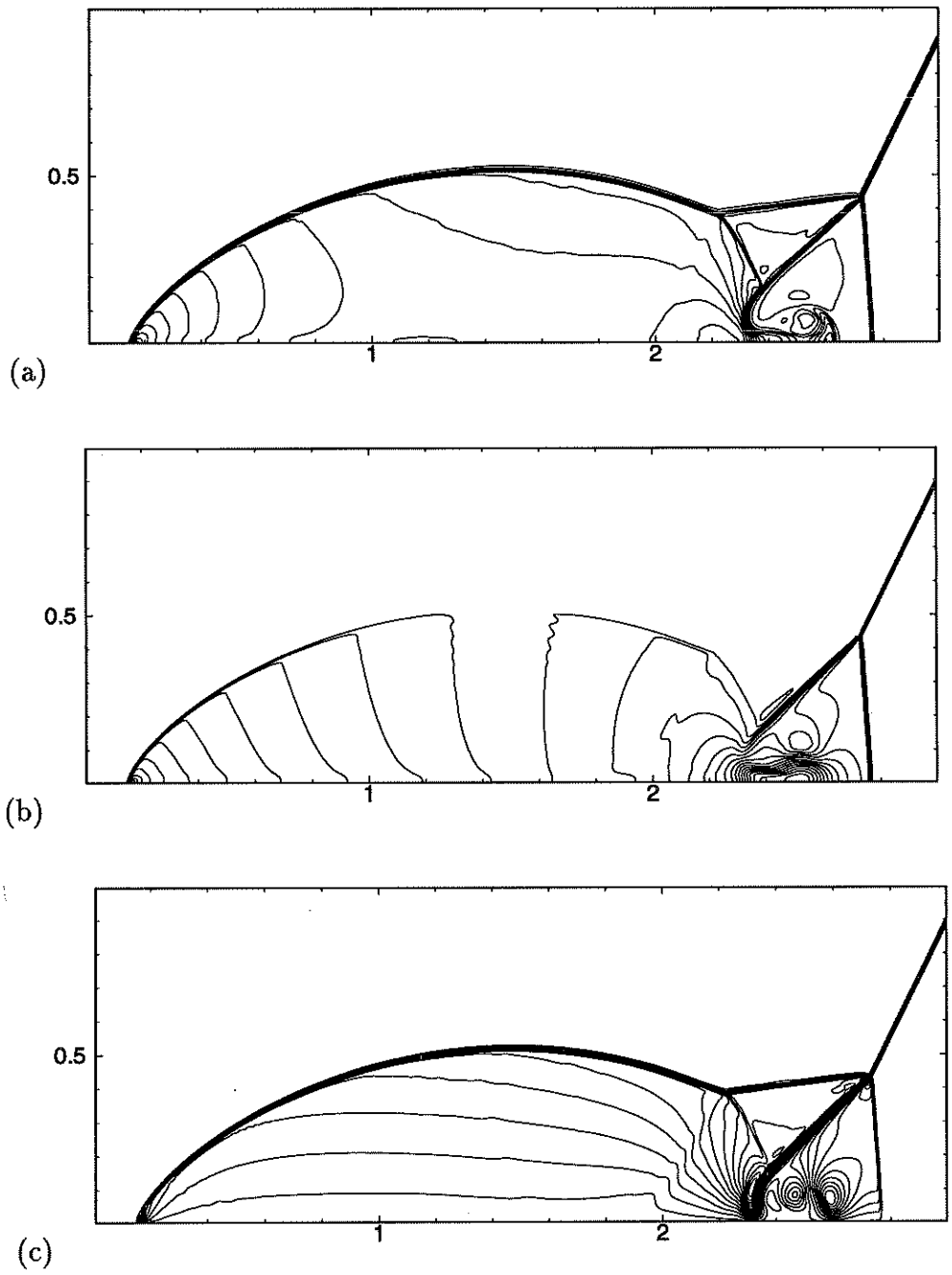

Figure 4.6: Double Mach reflection problem computed with the central scheme using UNO limiter with CFL=0.475 at $t = 0.2$ (a) density (b) x-velocity (c) y-velocity

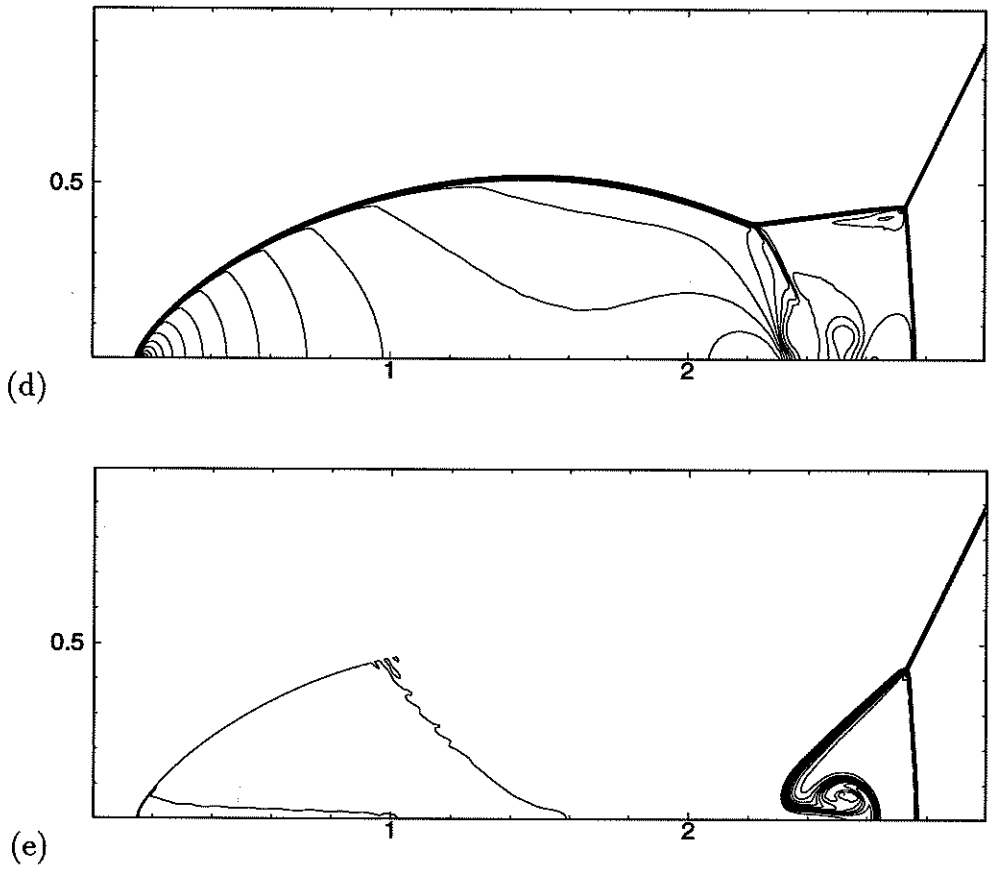

Figure 4.6: (cont'd) **Double Mach reflection problem computed with the central scheme using MM_2 limiter with CFL=0.475 at $t = 0.2$ (d) pressure (e) entropy**

A key feature of our central scheme is its *efficiency*, due to the fact that all the central computations reported below are free of the time-consuming characteristic decompositions and dimensional splitting. This in turn, is translated into *fast, simple*, 'two-lines' algorithm summarized in (2.15)-(2.16).
Table 4.2 quotes the CPU time, in seconds, for the computation of the two-dimensional Euler equations (4.3) subject to initial 'sine' density wave:

$$(\rho_0, u_0, v_0, p_0) = (1 + 0.2\sin(\pi(x+y)), 1, -0.5, 1).$$

We record the timing for two versions of the central scheme. The Jacobian-free version, which employs a straightforward *componentwise* computation of the discrete derivatives $f(w)'$ and $g(w)'$, and we compare it with the other version which utilizes the Jacobians $A = f_w$ and $B = g_w$ to compute the discrete derivatives of the fluxes, $f(w)' = Aw'$ and $g(w)' = Bw'$. We should emphasize that both versions yield comparable results, although as expected, the latter version using the explicit Jacobians performs with slightly better resolution. Which of the two versions is preferable depends on several factors:

- Whether the exact Jacobians are available. For example – gas-dynamics equation with *tabulated* pressure yields tabulated pointvalues of the flux (or requires an implicit computation of such); its Jacobians could only be interpolated.
- The specific hardware configuration. In this context we note that the Jacobian-free version requires, instead, additional computation of limiters (of the fluxes evaluated at the midvalues). Associated with these limiters are switches whose speed is configuration-dependent.
- The *size* of the computed system. Thus, for example, the computations of the larger 7×7 MHD systems reported in [TW], perform much faster with the Jacobian-free version.

N_s	N_t	MM_1 limiter	MM_2 limiter	UNO limiter	MM_1 limiter+ Artificial compression
CRAY C-90, with default compiler flags					
$f(w)' = Aw'$, $g(w)` = Bw`$					
200	100	2.69	3.22	3.43	4.06
400	200	20.38	24.76	26.47	32.44
$f(w)'$ and $g(w)`$ are obtained by componentwise limiters					
200	100	2.99	4.02	4.50	4.33
SUN Sparc20 (60MHz, SuperSparc), compiled with "-r8 -fast -O3"					
$f(w)' = Aw'$, $g(w)` = Bw`$					
100	50	10.79	14.29	16.28	18.30
200	100	92.27	119.13	136.98	159.26
$f(w)'$ and $g(w)`$ are obtained by componentwise limiters					
200	100	133.93	188.88	223.49	203.34

Table 4.2: CPU time in seconds for the central computation of the two-dimensional Euler system, with N_s cells in each spatial dimension and N_t temporal iterations, using various limiters.

4.3 Two-dimensional prologue — no dimensional splitting

Dimensional splitting, e.g., [RM], is an effective, widely used tool to solve multidimensional problems by piecing them from one-dimensional problems – one dimension at the time. Still, in the context of nonlinear conservation laws, dimensional splitting encounters several limitations; we refer, for example, to the important results of **Crandall & Majda** in [CM].

In this subsection we provide one more numerical evidence for the difficulties encountered with dimensional splitting, and with this we highlight the advantage of the our 'genuinely' multidimensional central scheme (2.15)-(2.16) to circumvent these difficulties. We consider the 2×2 system

$$\begin{pmatrix} u_1 \\ u_2 \end{pmatrix}_t + \begin{pmatrix} \frac{u_1^2}{\sqrt{u_1^2+u_2^2}} \\ \frac{u_1 u_2}{\sqrt{u_1^2+u_2^2}} \end{pmatrix}_x + \begin{pmatrix} \frac{u_1 u_2}{\sqrt{u_1^2+u_2^2}} \\ \frac{u_2^2}{\sqrt{u_1^2+u_2^2}} \end{pmatrix}_y = 0. \tag{4.4}$$

The system (4.4) was introduced by **Engquist & Runborg**, [ER], as part of a whole family of multi-phase modeling for geometrical optics expansions. The first member of this family, (4.4), represents a one-phase solution consisting of a single ray of strength $g(r,t) := \sqrt{u_1^2+u_2^2}$, located at a distance $r \equiv r(x,y)$ and an angle $\theta(x,y,t) := \arctan(u_2/u_1)$ relative to the (single) point source. We note that the system (4.4) is only *weakly* Hyperbolic in the sense that its linearized symbol contains a 2×2 Jordan block; this seems to play an essential role in the difficulties associated with the computation of this system by dimensional splitting methods.

Δx	Lax-Friedrichs(LxF) unsplitted		Lax-Friedrichs(LxF) splitted		Godunov splitted		Nessyahu-Tadmor(NT) splitted	
L^1 results:	error	order	error	order	error	order	error	order
1/10	0.0778	-	0.01268	-	0.1130	-	0.048	-
1/20	0.0433	0.85	0.01543	-0.28	0.065	0.8	0.0357	0.43
1/40	0.0229	0.92	0.01226	0.33	0.0404	0.69	0.0181	0.98
1/80	0.0118	0.96	0.0079	0.63	0.0235	0.78	0.00839	1.11
1/160	0.00599	0.98	0.00454	0.8	0.013	0.85	0.0039	1.11
L^∞ results:	error	order	error	order	error	order	error	order
1/10	0.949	-	0.0662	-	3.038	-	0.278	-
1/20	0.397	1.26	0.07	-0.79	2.911	0.062	0.235	0.25
1/40	0.171	1.21	0.056	0.32	2.867	0.022	0.191	0.3
1/80	0.0771	1.15	0.0369	0.6	2.834	0.017	0.0857	1.15
1/160	0.0363	1.09	0.0215	0.78	2.815	0.01	0.0589	0.54

Table 4.3: Accuracy of LxF , Godunov and NT (1.1)-(1.2) schemes (with and without dimensional splitting) for the one-phase geometric optics problem (4.4) at $t = 0.85$.

Following [ER], the system (4.4) is solved over the rectangle $0 \le x \le 1,\ 0 \le y \le 2$, subject to zero initial conditions (to avoid overflow, we initialize $u_1 = u_{2|t=0} \equiv 10^{-12}$). The system is then activated by exact inflow boundary conditions along the left boundary, $x = 0$: in this case, these boundary values were taken from an excat point source solution, $g(r,t) = \max(0,(t-r)^3)/r$, located at $(-0.2, 1)$.

In Table 4.3 we quote the numerical results from [ER] – the (fully) two-dimensional Lax-Friedrichs (LxF) scheme vs. the splitted versions based on the one-dimensional LxF scheme, Godunov scheme and NT scheme (1.1)-(1.2), which were complemented with dimensional splitting. Best results were obtained with the two-dimensional LxF scheme – the forerunner for all central schemes: the unsplitted version achieves (close to) the expected first-order accuracy in both L^1 and L^∞ norms. The following three 'splitted' versions which employ dimensional splitting, yield less accurate results. Indeed, a considerable loss of accuracy is observed with the splitted version of the LxF scheme[1]. The first-order upwind Godunov scheme, the forerunner for all upwind schemes, yields better L^1 errors; yet, measuring the L^∞ errors and consideration of the contour plots in [ER] show that the splitted version of Godunov scheme also *fails* to capture the full strength of the underlying computed rays. The same failure occurs with the splitted version of the second-order NT scheme: dimensional splitting causes the first-order L^1 errors and further loss of accuracy in terms of the L^∞ errors. In all three cases, this failure is attributed to the dimensional splitting.

These results should be contrasted with Table 4.4 where we quote the numerical results of the 'genuinely' two-dimensional central scheme (2.15)-(2.16) using the MinMod limiter, MM_2. Both versions – with and without the exact Jacobians, achieve close to the expected second accuracy. Figure 4.7 confirm the high-resolution of our central scheme.

Discrete derivatives...	N	L^∞ error	L^∞ order	L^1 error	L^1 order
$f(w)' = Aw'$ $g(w)` = Bw`$	20	2.27e-2	-	6.19e-4	-
	40	8.12e-3	1.48	2.14e-4	1.53
	80	2.97e-3	1.45	7.38e-5	1.54
	160	1.10e-3	1.43	1.97e-5	1.91
componentwise	20	2.83e-2	-	8.74e-4	-
	40	1.13e-2	1.32	2.89e-4	1.60
	80	4.51e-3	1.33	1.03e-4	1.49
	160	1.68e-3	1.42	2.86e-5	1.85

Table 4.4: Accuracy of the central approximation for the one-phase geometric optics problem (4.4) with MM_2 limiter.

[1] We thank Olof Runborg for these results

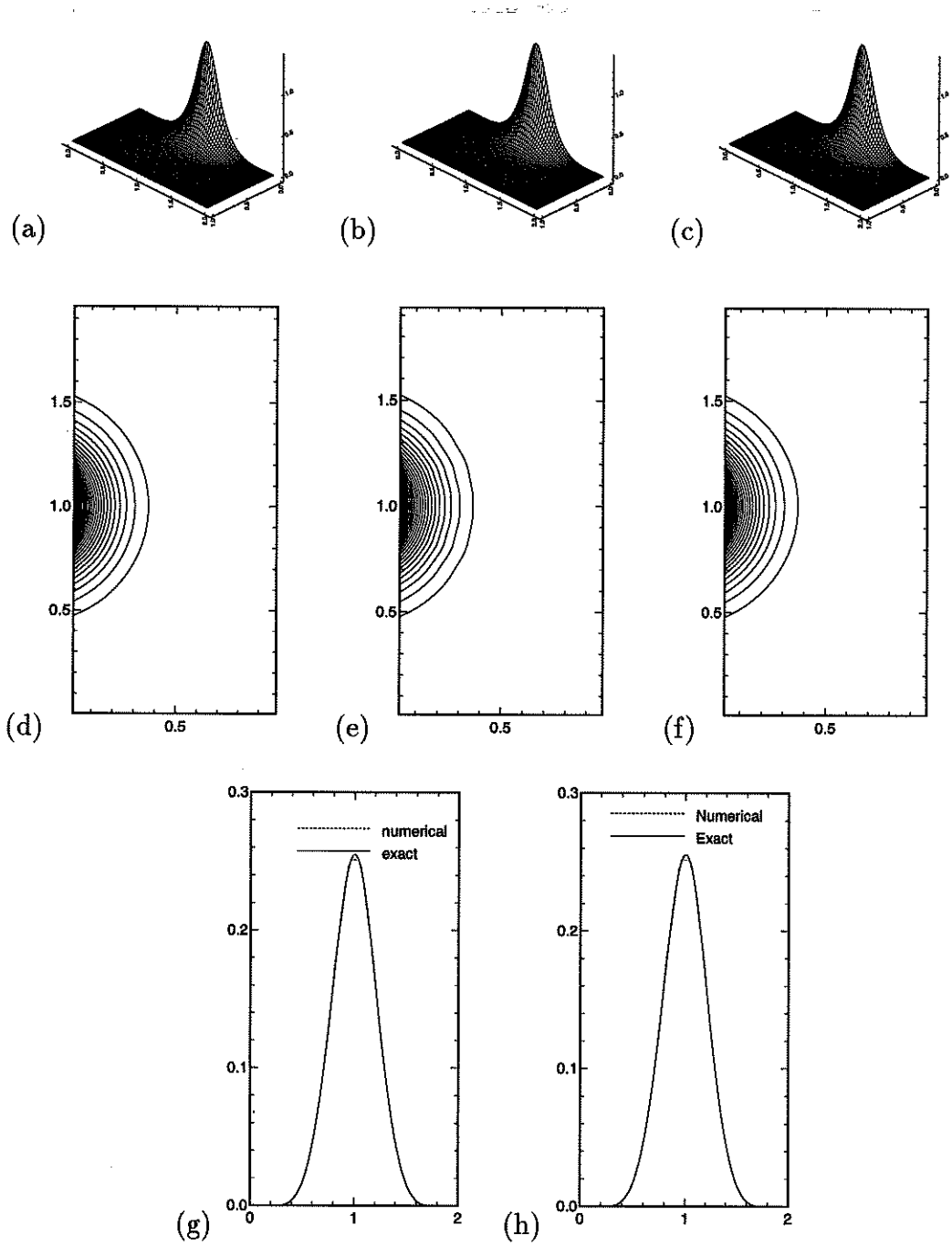

Figure 4.7: One-phase geometrical optics problem (4.4), computed by the two-dimensional central scheme with 40×80 cells and CFL=0.475 at $t = 0.85$. Ray strength of exact solution in (a) is compared with central scheme computation with MM_2 limiter in (b) and with UNO limiter in (c). Exact contour plot in (d) is compared with MM_2 and UNO limiters computations in (e) and (f), respectively. (g) and (h) are vertical cuts at $x = 0.2$ computed with MM_2 and UNO limiters.

5 Appendix – a central code for 2D-Euler equations

```
      subroutine EULER2D(nx,ny,dx,dy,cfl,gamma,theta,tf,tc,u)

*****************************************************************
* INPUT   nx, ny:  # of cells in x-, y-direction
*         dx, dy:  step size  in x-, y-direction
*         cfl:  CFL #;       gamma:  adiabatic constant of gas
*         theta:  constant parameter in the limiter (see (3.1))
*         tf:  final time to stop iteration;  tc:  current time
*         u:  conservative variables at time "tc"
*             entries of "u" needed: u(3:(nx+3),3:(ny+3),4)
* OUTPUT  u:  conservative variables after 2-stage time iteration
* REMARK  Reset parameters "nxm","nym" to adjust dimension of
*         arrays; Modify boundary conditions below when necessary.
* CAUTION u(i,j,*) when io=1 is on the cell with solid-line
*         in Figure 2.1, i.e. meaning u(i+1/2,j+1/2,*)
*****************************************************************

      parameter(nxm=408, nym=408, md=2, mn=4)
      real    u(0:nxm,0:nym,mn)
      real    f(0:nxm,0:nym,mn),  g(0:nxm,0:nym,mn)
      real   ux(0:nxm,0:nym,mn), uy(0:nxm,0:nym,mn)
      real   fx(0:nxm,0:nym,mn), gy(0:nxm,0:nym,mn)
      real bufx(0:nxm,0:nym),  bufy(0:nxm,0:nym)

      xmm(a,b) = 0.5*(sign(1.,a)+sign(1.,b))*min(abs(a),abs(b))
      xmm2(z,a,b) = xmm( z*xmm(a,b), 0.5*(a+b) )

      nxe = nx + md
      nye = ny + md

      gm1 = gamma - 1.0
      gm2 = 0.5 * gm1


*****************************************************************
* Start a 2-stage time iteration
      do io = 0, 1


* Periodic boundary condition in both x- & y-direction
      do m = 1, mn
      do i = 0, md
      do j = md + 1, nye
        u(i,      j,m) = u(nx+i,  j,m)
        u(nxe+i+1,j,m) = u(md+i+1,j,m)
      enddo
      enddo
      do j = 0, md
      do i = 0, nxe + md + 1
        u(i,j,      m) = u(i,ny+j,  m)
        u(i,nye+j+1,m) = u(i,md+j+1,m)
      enddo
      enddo
      enddo

* Compute numerical slopes for u in x- & y- direction
* (denoted as "ux" & "uy", resp.)
      do m = 1, mn
      do j = md - 2, nye + 2
      do i = md - 2, nxe + 2
        bufx(i,j) = u(i+1,j  ,m) - u(i,j,m)
        bufy(i,j) = u(i,  j+1,m) - u(i,j,m)
      enddo
      enddo
      do j = md, nye + 1
      do i = md, nxe + 1
        ux(i,j,m) = xmm2( theta, bufx(i-1,j), bufx(i,j) )
        uy(i,j,m) = xmm2( theta, bufy(i,j-1), bufy(i,j) )
      enddo
      enddo
      enddo

* Compute the fluxes f & g and maximum wave speeds
* in x- & y-direction (denoted as "em_x" & "em_y", resp.)
      em_x = 1.e-15
      em_y = 1.e-15
      do j = md - 2, nye + 3
      do i = md - 2, nxe + 3
        den = u(i,j,1)
        xmt = u(i,j,2)
        ymt = u(i,j,3)
        eng = u(i,j,4)
        vex = xmt / den
        vey = ymt / den
        pre = gm1 * eng - gm2 * den * ( vex * vex + vey * vey )
        cvel = sqrt( gamma * pre / den )
        em_x = max( em_x, abs(vex) + cvel )
        em_y = max( em_y, abs(vey) + cvel )
        f(i,j,1) = xmt
        f(i,j,2) = vex * xmt + pre
        f(i,j,3) = vex * ymt
        f(i,j,4) = vex * ( pre + eng )
        g(i,j,1) = ymt
        g(i,j,2) = vey * xmt
        g(i,j,3) = vey * ymt + pre
        g(i,j,4) = vey * ( pre + eng )
      enddo
      enddo

* Compute numerical slopes for f & g in x- & y- direction
* (denoted as "fx" & "gy", resp.)
      do m = 1, mn
      do j = md - 2, nye + 2
      do i = md - 2, nxe + 2
        bufx(i,j) = f(i+1,j  ,m) - f(i,j,m)
        bufy(i,j) = g(i,  j+1,m) - g(i,j,m)
      enddo
      enddo
      do j = md, nye + 1
      do i = md, nxe + 1
        fx(i,j,m) = xmm2( theta, bufx(i-1,j), bufx(i,j) )
        gy(i,j,m) = xmm2( theta, bufy(i,j-1), bufy(i,j) )
      enddo
      enddo
      enddo

* Compute the flux values of f & g at the center of the four faces
* (See Figure 2.2 & Eq. (2.15))
      do j = md, nye + 1
      do i = md, nxe + 1
        den = u(i,j,1) - dtodx2*fx(i,j,1) - dtody2*gy(i,j,1)
        xmt = u(i,j,2) - dtodx2*fx(i,j,2) - dtody2*gy(i,j,2)
        ymt = u(i,j,3) - dtodx2*fx(i,j,3) - dtody2*gy(i,j,3)
        eng = u(i,j,4) - dtodx2*fx(i,j,4) - dtody2*gy(i,j,4)
        vex = xmt / den
        vey = ymt / den
        pre = gm1 * eng - gm2 * den * ( vex * vex + vey * vey )
        f(i,j,1) = xmt
        f(i,j,2) = vex * xmt + pre
        f(i,j,3) = vex * ymt
        f(i,j,4) = vex * ( pre + eng )
        g(i,j,1) = ymt
        g(i,j,2) = vey * xmt
        g(i,j,3) = vey * ymt + pre
        g(i,j,4) = vey * ( pre + eng )
      enddo
      enddo

* Compute time step size
      if(io.eq.0) then
        dt = cfl / sqrt( (em_x/dx)**2 + (em_y/dy)**2 )
        if( ( tc + 2.*dt ) .ge. tf ) then
          dt = 0.5 * ( tf - tc )
        endif
      endif
      dtodx2 = 0.5 * dt / dx
      dtody2 = 0.5 * dt / dy
      tc = tc + dt

* Compute the values of "u" at the next time level (see (2.16))
      do m = 1, mn
      do j = md + 1 - io, nye - io
      do i = md + 1 - io, nxe - io
        bufx(i,j) =0.25 * (  u(i,j,  m) +  u(i+1,j,  m)
     &                     +  u(i,j+1,m) +  u(i+1,j+1,m) )
     &          + 0.0625 * ( ux(i,j,  m) - ux(i+1,j,  m)
     &                     + ux(i,j+1,m) - ux(i+1,j+1,m)
     &                     + uy(i,j,  m) + uy(i+1,j,  m)
     &                     - uy(i,j+1,m) - uy(i+1,j+1,m) )
     &          + dtodx2 * (  f(i,j,  m) -  f(i+1,j,  m)
     &                     +  f(i,j+1,m) -  f(i+1,j+1,m) )
     &          + dtody2 * (  g(i,j,  m) +  g(i+1,j,  m)
     &                     -  g(i,j+1,m) -  g(i+1,j+1,m) )
      enddo
      enddo
      do j = md + 1, nye
      do i = md + 1, nxe
        u(i,j,m) = bufx(i-io,j-io)
      enddo
      enddo
      enddo


      enddo
* End of the 2-stage time iteration
*****************************************************************

      return
      end
```

References

[AV] P. Arminjon and M.C. Viallon, *Généralisation du schéma de Nessyahu-Tadmor pour une équation. hyperbolique à deux dimensions d'espace*, C.R. Acad. Sci. Paris, t. 320, série I. 1995, p. 85-88.

[BS] F. Bereux and L. Sainsaulieu, *A higher order method for the solution of Hyperbolic systems with relaxation*, Preprint.

[CM] M. Crandall and A. Majda, *The method of fractional steps for conservation laws*, Numer. Math. 34 (1980), pp. 285-314.

[CW] P. Colella and P. Woodward, *The piecewise parabolic method (PPM) for gas-dynamical simulations*, JCP **54**, 1984, pp. 174-201.

[Er] Erbes, *A high-resolution Lax-Friedrichs scheme for Hyperbolic conservation laws with source term. Application to the Shallow Water equations.* Preprint.

[EO] B. Engquist and S. Osher, private communication.

[ER] B. Engquist and O. Runborg, *Multi-phase computations in geometrical optics*, J. Comp. Appl. Math., 1996, in press.

[Go] S.K. Godunov, *A finite difference method for the numerical computation of discontinuous solutions of the equations of fluid dynamics*, Mat. Sb. **47**, 1959, pp. 271-290.

[Ha1] A. Harten, *The artificial compression method for the computation of shocks and contact discontinuities:I. single conservation laws*, CPAM 39 (1977), pp. 611-638.

[Ha2] A. Harten, *High resolution schemes for hyperbolic conservation laws*, JCP **49**, 1983, pp. 357-393.

[HEOC] A. Harten, B. Engquist, S. Osher and S.R. Chakravarthy, *Uniformly high order accurate essentially non-oscillatory schemes. III*, JCP **71**, 1982, pp. 231-303.

[HO] A. Harten and S. Osher, *Uniformly high order accurate non-oscillatory scheme. I*, SINUM **24**, 1982, pp. 229-309.

[Hu] Huynh, *A piecewise-parabolic dual-mesh method for the Euler equations*, AIAA-95-1739-CP, The 12th AIAA CFD Conf., 1995.

[JS] G.-S Jiang and C.-W. Shu, *Efficient implementation of weighted ENO schemes*, JCP.

[JX] S. Jin and Z. Xin, *The relaxation schemes for systems of conservation laws in arbitrary space dimensions*, CPAM **48**, 1995, pp. 235-276.

[La] P.D. Lax, *Weak solutions of non-nonlinear hyperbolic equations and their numerical computations*, CPAM **7**, 1954, pp. 159-193.

[Le] B. van Leer, *Towards the ultimate conservative difference scheme, V. A second order sequel to Godunov's method*, JCP **32**, 1979, pp. 101-136.

[LL] X.-D. Liu and P. D. Lax "Positive Schemes for Solving Multi-dimensional Hyperbolic Systems of Conservation Laws," *Courant Mathematics and Computing Laboratory Report,* NYU, 95-003(1995), and submitted to CPAM.

[LO] X.-D. Liu and S. Osher, *Non-oscillatory high order accurate self similar maximum principle satisfying shock capturing schemes. I*, SINUM **33**, 1996, in press.

[LT] X.-D. Liu and E. Tadmor, *Third order non-oscillatory central scheme for Hyperbolic conservation laws*, UCLA preprint.

[MO] A. Majda and S. Osher, *Propagation of error into regions of smoothness for accurate difference approximations to hyperbolic equations*, CPAM 30 (1977), pp. 671-705.

[NT] H. Nessyahu and E. Tadmor, *Non-oscillatory central differencing for hyperbolic conservation laws*, JCP **87**, 1990, pp. 408-448.

[NTT] H. Nessyahu, E. Tadmor and T. Tassa, *On the convergence rate of Godunov-type schemes*, SINUM **31**, 1994, pp. 1-16.

[OT] S. Osher and E. Tadmor, *On the convergence of difference approximating to scalar conservation laws*, Math. Comp., **50**, 1988, pp. 15-51.

[Ro] P. Roe, *Approximate Riemann solvers, parameter vectors, and difference schemes*, JCP **43**, 1981, pp. 357-372.

[RM] R.D. Richtmyer and K.W. Morton, **Difference Methods for Initial Value Problems**, 2nd ed., New-York, Interscience, 1967.

[Sa1] R. Sanders, *A third-order accurate variation non-expansive difference scheme for single conservation laws*, Math. Comp. **51**, 1988, 535-558.

[Sa2] R. Sanders, Private communication.

[SW] R. Sanders and A. Weiser, *A high resolution staggered mesh approach for nonlinear hyperbolic systems of conservation laws*, JCP **1010**, 1992, pp. 314-329.

[Sw] P. Sweby, *High resolution schemes using flux limiters for Hyperbolic conservation laws*, SINUM **5**, 1984, pp. 995-1011.

[Sh] C.-W. Shu, *Numerical experiments on the accuracy of ENO and modified ENO schemes*, JCP **5**, 1990, pp. 127-149.

[So] G. Sod, *A survey of several finite difference methods for systems of nonlinear hyperbolic conservation laws*, JCP **22**, 1978, pp. 1-31.

[TW] E. Tadmor and C.C. Wu, *Central scheme for the multidimensional MHD equations*, in preparation.

[WC] P. Woodward and P. Colella, *The numerical simulation of two-dimensional fluid flow with strong shocks*, JCP **54**, 1988, pp. 115-173.